

Grant Agreement No.: 318600

SODALES

Software-Defined Access using Low-Energy Subsystems

Funding Scheme: ***Small or medium-scale focused research project STREP - CP-FP-INFSO***
Activity: **ICT-8-1.1 - Future Networks**

D4.2 Prototype implementation and lab validation

Due date of the Deliverable: Month 28
Actual submission date: 9th July 2015
Start date of project: November 1st 2012 Duration: 36 months
Project Manager: Carlos Bock | i2CAT
Version: 1.0

Author List: Michael Parker, Geza Koczis, Terry Quinlan, Stuart Walker (UEssex), Jordi Ferrer, Carlos Bock (i2CAT), Volker Jungnickel, Dominic Schulz (HHI), Victor Marques (PTI), David Levi (Ethernity)

Project co-funded by the European Commission in the 7 th Framework Programme (2007-2013)		
Dissemination Level		
PU	Public	✓
PP	Restricted to other programme participants (including the Commission Services)	
RE	Restricted to a group specified by the consortium (including the Commission Services)	
CO	Confidential, only for members of the consortium (including the Commission Services)	

	<i>Deliverable D4.2</i>	<table><tr><td>Project</td><td>SODALES</td></tr><tr><td>Doc</td><td>D4.2 Prototype implementation and lab validation</td></tr><tr><td>Date</td><td>9/07/2015</td></tr></table>	Project	SODALES	Doc	D4.2 Prototype implementation and lab validation	Date	9/07/2015
Project	SODALES							
Doc	D4.2 Prototype implementation and lab validation							
Date	9/07/2015							

Abstract

This deliverable D4.2, “SODALES prototype lab verification report” describes the results on the laboratory validation tests of the wireless (optical and mm-wave) technologies envisioned for the multi-Gb/s final-drop links between active remote node (ARN) and end-user customer premises equipment (CPE), for small-to-medium sized enterprises (SMEs) and/or domestic locations.

Results for 60 GHz, 24 GHz, and optical wireless (OW) systems are presented, as is a 5-Gb/s custom solution for converged fixed-mobile (5G) networking. In addition, the Fault Management implementation for the Control and Management Plane are presented.

The technologies discussed in this D4.2 deliverable are being fed into the final validation and commercial field trials of the SODALES project.

Document Revision History

Version	Date	Description of change	Authors
1.0	9/7/2015	Final Version	Michael Parker, Geza Koczis, Terry Quinlan, Stuart Walker, Jordi Ferrer, Carlos Bock, Volker Jungnickel, Dominic, Schulz, Victor Marques, David Levi


	<i>Deliverable D4.2</i>	<table><tr><td>Project</td><td>SODALES</td></tr><tr><td>Doc</td><td>D4.2 Prototype implementation and lab validation</td></tr><tr><td>Date</td><td>9/07/2015</td></tr></table>	Project	SODALES	Doc	D4.2 Prototype implementation and lab validation	Date	9/07/2015
Project	SODALES							
Doc	D4.2 Prototype implementation and lab validation							
Date	9/07/2015							

Table of Contents

1	Introduction	1
2	Final-Drop Technologies	3
2.1	Optical fixed links	3
2.1.1	Introduction	3
2.1.2	Throughput and latency measurements	4
2.1.3	Initial field experiments	7
2.2	Mm-wave fixed links	14
2.2.1	Introduction	14
2.2.2	IEEE 802.11ac	16
2.2.3	24 GHz Wireless	18
2.2.4	802.11ad and WiGig	19
2.2.5	802.11ac and 802.11ad implementation and suitability for multi-gigabit use	21
2.2.6	Experimental results	22
2.2.7	5 Gbit/s Realtime Baseband Processing	30
	Conclusions and further work	35
3	Control & Management Platform	37
3.1	Fault Management	37
3.1.1	Active Remote Node	37
3.1.2	Customer Premises Equipment	44
4	Conclusions	46
5	References	47

Figure Summary

Figure 1: Configuration for throughput measurements.....	4
Figure 2: Setup for net throughput and latency measurements.....	4
Figure 3: Left: Data rate (gross) as a function of transmission range, Right: Data rates (gross) as a function of SNR Inset: Configuration of the OW system - LOS Tx lens 3" f=10cm, Rx lens 3" f=8.5cm, IR LED 24°.....	5
Figure 4: Net throughput as a function of the transmitting frame size for different average SNR per carrier.....	6
Figure 5: Average latencies for different possible throughputs $Th(\alpha)$ without (red) and with (blue) emulated flow control.	6
Figure 6: Next generation chipset, solid lines: average latencies w/ emulated FC; dashed line: average latencies w/o emulated FC and dotted line: net data rate for different frame sizes.	7
Figure 7: Left: Optical wireless transceiver prepared for outdoor trials. Right: Campus map of TUB where the link is installed (source Google Earth/Berlin 3D).	8
Figure 8: Recorded Visibility (red) and data rate (blue) for the OW link (top) as compared to the FSO link data rates (green curve, bottom) during a dense fog event.	9
Figure 9: Despite high visibility (red curve) reduced data rates for the OW link (blue curve) are observed for several hours due to sunlight scattered by clouds.....	10
Figure 10: Cumulative distribution function of the observed data rate (left) and the visibility (right).....	11
Figure 11: Historical 802.11 PHY data rate improvement.....	15
Figure 12: Different MIMO concepts: a) SU-MIMO beamforming; b) downlink MU-MIMO beamforming.....	17
Figure 13: Example of downlink MU-MIMO.....	17
Figure 14: Data channels for 802.11ac in Europe.....	18
Figure 15: Specific attenuation for atmospheric oxygen and water vapour.....	19
Figure 16: Worldwide frequency allocation at 60 GHz band.....	20
Figure 17: Example scenario of 802.11ad [14].....	22
Figure 18: 802.11ac point-to-point experimental results.	23
Figure 19: GHz back-to-back set-up in full duplex operation [23].....	24
Figure 20: (a) Active antenna, (b) Wireless card [24].....	25
Figure 21: Omnidirectional antenna basic characterisations (left: 90° azimuth directivity, right: 330° azimuth directivity).....	25
Figure 22: Live streaming of 4K UHD TV signals over 802.11ad.....	26
Figure 23: (a) Antenna structure, and (b) Patch feed points.....	27
Figure 24: (a) Port 1 excited for horizontal polarization. (b) Port 2 excited for vertical polarization.	27
Figure 25: 5 GHz H/V polarization patch and MMIC switch.	28
Figure 26: 60 GHz semi-rigid slot antenna [26].....	28
Figure 27: Copolar E-plane radiation patterns at 60 GHz (corresponding crosspolar radiation patterns inset): (a) top view and (b) side view.....	29
Figure 28: Real-time transceiver building blocks.....	31
Figure 29: Frame synchronisation using the serial Schmidl-Cox algorithm of a continuous data stream.....	32


	<i>Deliverable D4.2</i>	<table><tr><td>Project</td><td>SODALES</td></tr><tr><td>Doc</td><td>D4.2 Prototype implementation and lab validation</td></tr><tr><td>Date</td><td>9/07/2015</td></tr></table>	Project	SODALES	Doc	D4.2 Prototype implementation and lab validation	Date	9/07/2015
Project	SODALES							
Doc	D4.2 Prototype implementation and lab validation							
Date	9/07/2015							

Figure 30: BER simulation with and w/o DC-compensation (left w/o scrambler, right with scrambler)	33
Figure 31: Setups for packet loss ratio (a, cont. lines), EVM (left, dashed) and SNR vs BER (b) measurements	33
Figure 32: Constellation plot and EVM results (l.), Bit Error Ratio vs Signal to Noise Ratio (r.) ...	34
Figure 33: Notifications logging view from the unified management plane	39
Figure 34: Equipment boards, board status view	40
Figure 35: Switch fabric status.....	41
Figure 36: Lag Interfaces status	42
Figure 37: Services list	42
Figure 38: CFM configuration at the ENET CPEs	45


Table Summary

Table 1: Parameters of the current OW link.....	12
Table 2: Optimized key parameters	13
Table 3: Basic technology parameters for 802.11ac and 802.11ad	15
Table 4: Channel numbers in the 60 GHz band.....	21
Table 5: Attenuation of various building materials.....	24
Table 6: Ethernet protocol analyser results.....	35

List of Acronyms

ADC	Analogue-to-Digital Converter
AP	Access Point
ARN	Active Remote Node
BER	Bit Error Rate
CDF	Cumulative Distribution Function
CFM	Connectivity Fault Management
CMOS	Complementary Metal Oxide Semiconductor
CPE	Customer Premises Equipment
CRC	Cyclic Redundancy Check
DAC	Digital-to-Analogue Converter
D2D	Device-to-Device
D2I	Device-to-Infrastructure
DC	Direct Current
DQPSK	Differential Quadrature Phase Shift Keying
EVM	Error Vector Magnitude
FC	Flow Control
FDD	Frequency-Division Duplex
FEC	Forward Error Correction
FOV	Field of View
FPGA	Field Programmable Gate Array
FSO	Free-Space-Optical
FWHM	Full-Width Half-Maximum
GE	Gigabit Ethernet
HDD	Hybrid Division Duplex
HSPA	High-Speed Packet Access
IR	Infra Red
LAN	Local Area Network
LED	Light Emitting Diode
LFSR	Linear Feedback Shift Register
LOS	Line of Sight
LTE	Long-Term Evolution
MAC	Media Access Control
MIMO	Multiple-Input Multiple-Output
MU	Multiple User
NMS	Network Management System
NLOS	Non Line of Sight
OFDM	Orthogonal-Frequency-Division Multiplexing
OLT	Optical Line Termination
ONT	Optical Network Termination
OW	Optical Wireless
PD	Photodiode
PHY	Physical layer
QPSK	Quadrature Phase Shift Keying
RF	Radio Frequency
RRC	Root-Raised Cosine
SC	Single Carrier

SNR Signal to Noise Ratio
SU Single User
TDD Time-Division Duplex
VLAN Virtual Local Area Network
VLC Visible Light Communications
WLAN Wireless Local Area Network

	<i>Deliverable D4.2</i>	<table><tr><td>Project</td><td>SODALES</td></tr><tr><td>Doc</td><td>D4.2 Prototype implementation and lab validation</td></tr><tr><td>Date</td><td>9/07/2015</td></tr></table>	Project	SODALES	Doc	D4.2 Prototype implementation and lab validation	Date	9/07/2015
Project	SODALES							
Doc	D4.2 Prototype implementation and lab validation							
Date	9/07/2015							


1 Introduction

In this deliverable D4.2 “Prototype lab verification report” we present results on the laboratory validation tests on the key technologies being developed in the SODALES project. Principally the wireless (optical and mm-wave based) interfacing technologies potentially offering high capacity (1-10 Gb/s) final-drop links between the ARN and the end-users (domestic customers and SME business users); and the Control & Management Plane system based on the OpenNaaS tool set, in particular the fault management platform for both the ARN and CPE parts of the SODALES architecture. With regard to ARN switching, this was already reported upon in the earlier deliverable D4.1, whilst software simulations for the C&M plane have been extensively reported upon in the parallel deliverables of WP3. This deliverable D4.2 also follows on from the earlier deliverable D4.1, which provided the prototype specifications as well as the HW/SW interface specifications for the SODALES architecture.

Although primarily researched in the context of the SODALES project, the technologies reported here have also been developed and tested with future 5G networking applications in mind, although the SODALES project wasn’t conceived originally as a 5G architecture; however, its innovative converged architecture makes it an important precursor technology solution towards 5G networking, which makes the results presented here of particular relevance, e.g. to latest research projects involved in the H2020 5G-PPP programme, in which all the partners in the SODALES project are also now engaged. This simply underlines the relevance of the SODALES project results for the ongoing 5G research initiative, even after the project concludes at the end of October 2015.

Millimetre-wave technology solutions are reported in this deliverable, offering multi-Gb/s data capacities. Two standards (IEEE 802.11ac and IEEE 802.11ad) have been proposed for 60 GHz short range communications, suitable for the ARN-CPE final-drop link, with the 802.11ad standard making use of directional antennas and beamforming to enhance link quality and modify channel access to address directionality and spatial reuse. The relatively limited range of 60 GHz enhances frequency reuse which might even augment overall wireless security because eavesdroppers outside a given installation will have a much more difficult time grabbing 60 GHz signal. The 24 GHz spectrum results described here also delivered full-duplex data rates of beyond 1 Gb/s in non line of sight (NLOS) conditions. It was demonstrated that gigabit throughput using the 24-GHz frequency band is also an option for future in-building wireless networks.

A 5 Gbit/s custom solution for future mm-wave converged fixed-mobile networks is also reported in this deliverable, based on FPGA technology and comprising two parallel complex-valued data channels in each direction together with a standard 10G Ethernet interface. A DSP function to compensate for a lower cut-off frequency of 4.5 MHz has been simulated and implemented, and is reported here, whilst a serial Schmidl-Cox algorithm performing frame synchronisation for a 2.5 GSa/s data stream is demonstrated. EVM values below -30 dB for the transmitter output


	<i>Deliverable D4.2</i>	<table><tr><td>Project</td><td>SODALES</td></tr><tr><td>Doc</td><td>D4.2 Prototype implementation and lab validation</td></tr><tr><td>Date</td><td>9/07/2015</td></tr></table>	Project	SODALES	Doc	D4.2 Prototype implementation and lab validation	Date	9/07/2015
Project	SODALES							
Doc	D4.2 Prototype implementation and lab validation							
Date	9/07/2015							

signal were achieved and the required SNR for an error-free transmission was about 15.5 dB. On the Ethernet layer all frames could be transmitted without CRC or other errors.

A low-cost rate adaptive optical wireless (OW) system with a peak gross data rate of 500 Mb/s is also described in this deliverable D4.2, for use as a final-drop technology for the SODALES architecture, or as a backhaul link for small mobile radio cells. An initial long-term outdoor trial was performed using this technology, with a 100-m link distance monitored over the five winter months to observe the influence of bad weather conditions. Initial results indicate that the optical wireless data-rate is higher than 100, 39 and 22 Mb/s for 72, 99 and 99.9 % of the time, respectively; whilst the lowest observed data rate due to intemperate weather conditions was 9 Mb/s. Visibilities lower than 200 m were never observed even for the worst weather conditions, which leads to unprecedented availability, at least over short distances. A link simulation model was developed and reported here, with the key parameters modified to indicate that it is possible to achieve 1 Gb/s per wavelength over 100 m distance.

Finally, we briefly report on the features of the control and management platform implementing basic fault management within the SODALES architecture for both the ARN and the CPE devices. Fault management at the CPE is implemented in accordance with the elemental Connectivity Fault Management (CFM) features specified in the IEEE 802.1ag standard, which also emphasizes usage of CFM for Metro Ethernet services.

Overall, many of the technologies reported in this deliverable D4.2 are being deployed in the final SODALES demonstrators (both validation and commercial field trials), which are described in greater detail in the parallel deliverable D4.3 “Report on installation parameters for the field service validation”, and which will also be finally reported upon in the concluding deliverable D4.4 “Report on lab and field service validation” of WP4. Thus the work reported here is being fed into the final tasks of the project for a successful and commercially-interesting conclusion to the SODALES enterprise.

	<i>Deliverable D4.2</i>	<table><tr><td>Project</td><td>SODALES</td></tr><tr><td>Doc</td><td>D4.2 Prototype implementation and lab validation</td></tr><tr><td>Date</td><td>9/07/2015</td></tr></table>	Project	SODALES	Doc	D4.2 Prototype implementation and lab validation	Date	9/07/2015
Project	SODALES							
Doc	D4.2 Prototype implementation and lab validation							
Date	9/07/2015							

2 Final-Drop Technologies

2.1 Optical fixed links

2.1.1 Introduction

SODALES has a clear application scenario for the use of optical fixed links in a line-of-sight deployment scenario between the ARN and end-users, e.g. for domestic and/or small industry connectivity. Alongside this technology trend, we are also currently experiencing the roll-out of LTE fourth generation (4G) mobile radio, with the result that alongside the base coverage provided by the macro-cells, an overall higher network capacity is being reached by the addition of small cells at locations where the traffic density is high [1], thus increasing the local density of base stations. The deployment of such small cells also needs the appropriate economic backhaul technology solutions, which can also be addressed by optical fixed link technology.

Optical wireless (OW) offers such high capacity without the need for RF spectrum. At the typical distances below 100 m for the backhaul of small cells, OW is an attractive approach because bad visibility is considered harmless and thus availability is high [2]. The probability of a free line-of-sight (LOS) increases if the distance is reduced.

Visible light communication (VLC) has also attracted high interest recently, where low-cost high-power LEDs used for lighting can be modulated at high speed, with recent research demonstrating data rates of several Gbit/s [3].

In this context, we have been able to modify recent VLC technology to set up an OW link to demonstrate the applicability for the low cost backhaul of small cells. These are usually deployed at lamp-post height, within 50 to 100 m of the macro cell sites which are typically at rooftop level.

Modern VLC links use orthogonal-frequency-division multiplexing (OFDM) and real-time closed-loop link adaptation [3], such that the throughput can be adapted to the link distance and weather conditions, as opposed to the classical approach to OW links that simply provides a fixed data rate. Such link adaptation improves availability and for all practical purposes, it is becoming mandatory as a means to enable realistic backhaul deployment.

This new approach raises three immediate questions, which have to be answered.

1. Can the ray from a LED be optimized so that a sufficient throughput for small cell backhauling is reached?
2. Considering that closed-loop transmission is needed for link adaptation, is the latency low enough for recent mobile network technologies such as High-Speed Packet Access (HSPA) and LTE?
3. What is the availability of such optical wireless links when used in a real deployment scenario?

2.1.2 Throughput and latency measurements

In order to provide some answers to these important questions, we have performed some outdoor laboratory trials, to assess the performance of the optical wireless technology for fixed final-drop applications. For all measurements, a real-time OW link with 500 Mbit/s peak gross rate was used, including a single low-cost infrared LED SFH 4783 with an active area of $1 \times 1 \text{ mm}^2$ [3][4]. The LED uses an optical concentrator to yield 25° divergence full width at half maximum (FWHM).

2.1.2.1 Setup for throughput measurements

The OW transmitter was further equipped with a 3" lens with 100 mm focal length to reduce the beam width to 4° FWHM. The lens creates a magnified image of the radiation plane of the LED in the receiver plane. E.g. at 50 m distance, the magnification ratio is 7×500 , where the first and the second factor are due to the concentrator and the lens, respectively. At this distance, the $7 \times 7 \text{ mm}^2$ LED chip illuminates an area of $3.5 \times 3.5 \text{ m}^2$ nearly homogeneously. Such a large illumination area is highly beneficial for the practical deployment and resilience of the technology. It makes the link robust and corrects small pointing errors at the lamp post. At the receiver, a 3" lens with $f = 85 \text{ mm}$ was used in combination with a silicon photodiode S6968 of 14 mm diameter. Figure 1 shows the setup for the data rate measurements.

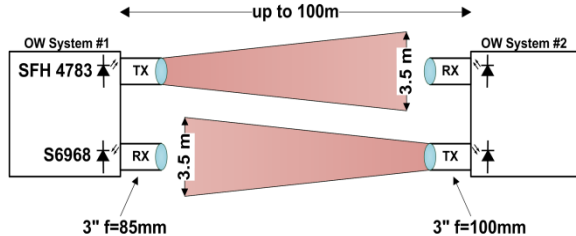


Figure 1: Configuration for throughput measurements

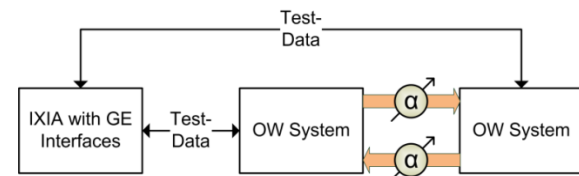


Figure 2: Setup for net throughput and latency measurements

The receiver field of view (FOV) is 9° and hence wider than the transmitter beam width. Alignment is simply done by pointing the transmitter to the receiver, and it is supported by an add-on telescope that is removed after the link is installed.

2.1.2.2 Setup for latency measurements

Besides the data rate requirements for LTE small cell backhauling, there are also requirements concerning latency. The recommended end-to-end latency for an X2 LTE backhaul is 10 ms [5]. The X2 link is important for communication between base stations, e.g. during hand-over.

As OW performance will tend to be impaired in poor visibility conditions [2], a stable and uninterrupted data link can be realized by adapting the data rate accordingly. We have tested latency at variable visibility with a standard Ethernet RFC 2544 latency test using different attenuation values. Figure 2 shows the experimental setup using an IXIA XM12 Protocol Tester equipped with two Gigabit Ethernet (GE) interfaces.

The OW system integrates an adaptive real-time baseband signal processing and a GE interface for application data. The impact of rate adaptation onto latency is studied by increasing the attenuation α and thereby reducing the signal-to-noise ratio (SNR). In this way, the maximum possible transmission rate $Th(\alpha)$ in the optical link is modified.

2.1.2.3 Results

Throughput

The achievable data rate depends almost linearly on the received optical power and thereby on the SNR at the receiver. The path loss can be modified by means of intensity and aperture at the receiver site [3].

Measurements for the data rate vs. distance and SNR are shown in Figure 3. While for short distance and high SNR, a gross rate of 465 Mbit/s was achieved, throughput is reduced for larger distances and smaller SNRs. At the relevant distances of 50 and 100 m for small-cell backhauling, a throughput of 280 and 120 Mbit/s was measured, respectively. The highest bitrate-distance product of 14 Gbit/s·m was thus obtained over a 50 m link length. To our best knowledge, this is the highest bitrate-times-distance product ever demonstrated with a real-time rate-adaptive optical wireless system.

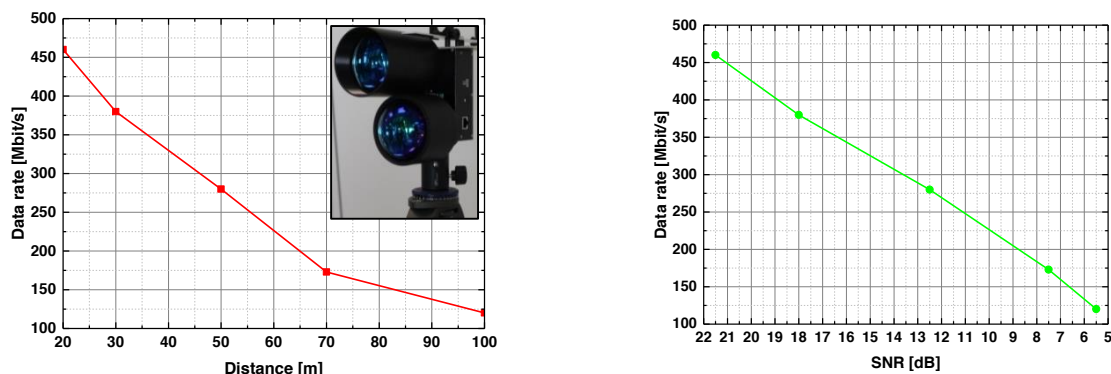


Figure 3: Left: Data rate (gross) as a function of transmission range, Right: Data rates (gross) as a function of SNR Inset: Configuration of the OW system - LOS Tx lens 3" f=10cm, Rx lens 3" f=8.5cm, IR LED 24°

Latency

Figure 5 shows that the net throughput is smaller in general for smaller frame sizes, which is attributed to the fact that there is a higher overhead relative to the payload of a smaller frame size. Moreover, a higher number of smaller packets must be processed. Most likely, there are limits of the signal-processing engine reducing the total data rate for small packets. The maximum throughput $Th(\alpha)$ is reached at packet sizes of 512 bytes and greater, and for all SNR values. The average SNR per carrier is given in the legend of Figure 4.

Next, latency was studied as a function of $Th(\alpha)$ and frame size for constant SNR. Initially, the latency test was conducted using 100% of the maximal throughput $Th(\alpha)$. Starting from small

packet sizes, at first a low latency of around 10 ms was measured until the packet size reached the point where $Th(\alpha)$ is reached. From this packet size the latency starts to be increasingly proportional to the frame size, yielding a maximum latency as large as 140 ms, as shown in Figure 5. However, these large values are not typical for normal network operation.

When a net throughput of 100% of $Th(\alpha)$ is reached, obviously, queues start to fill and the latency is increased. The rising latency is related to the implementation of the RFC 2544 test in our protocol tester, which always provides a fixed data rate and thus ignores the fact that flow control is typically used at layer 2. In a real system, if 100% of $Th(\alpha)$ is reached, congestion is avoided by reducing the source rate. Flow control is used in any network card, and this needs to be considered in order to get realistic latency results.

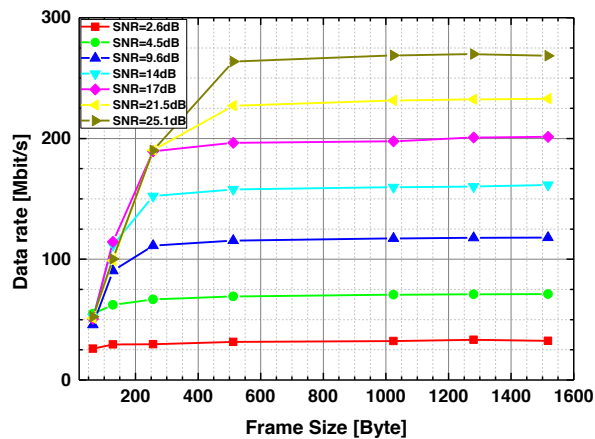


Figure 4: Net throughput as a function of the transmitting frame size for different average SNR per carrier

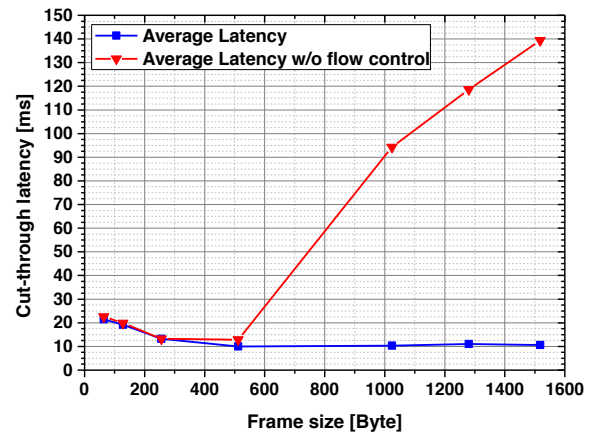


Figure 5: Average latencies for different possible throughputs $Th(\alpha)$ without (red) and with (blue) emulated flow control.

Flow control was emulated here by reducing the data rate in the RFC 2544 test to 95% of $Th(\alpha)$ and then performing the latency measurements once again. It can be observed in Figure 5 that the overall average latency is significantly lower at $10 \text{ ms} \pm 1 \text{ ms}$ for frame sizes larger than 512 bytes, once flow control has been emulated. Moreover, latency is now found to be independent of the average SNR.

The measurements discussed above were also performed again with a next-generation chipset. First of all, the net throughput was found to be 230% higher due to the different physical layer parameters. Similarly to before, throughput is reduced at the smaller frame sizes, as illustrated in Figure 6 (dotted line); however, the penalty is notably smaller than as compared with the chipset that is in current use.

At a frame size of 512 bytes, 100% of $Th(\alpha)$ is reached and again, the latency grows because the frames are put into queues due to the congestion. However, the latency is significantly smaller in general; the value of around 2 ms rises to a maximum value not larger than 31 ms. Afterwards, measurements with emulated FC were conducted in the same way as described above. Relative

to the currently used chipset, latency is reduced by 80% to around $2 \text{ ms} \pm 1 \text{ ms}$, see Figure 6 (solid line).

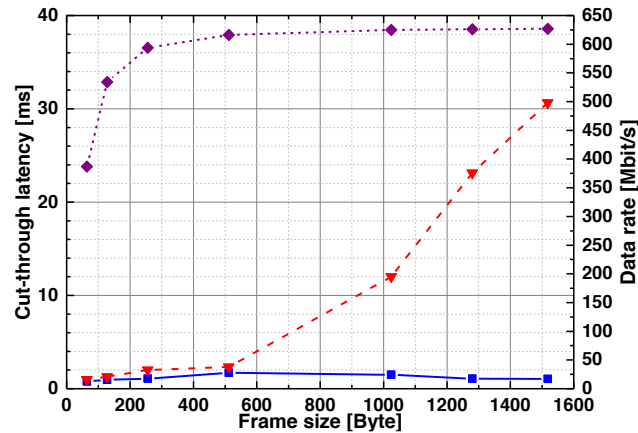


Figure 6: Next generation chipset, solid lines: average latencies w/ emulated FC; dashed line: average latencies w/o emulated FC and dotted line: net data rate for different frame sizes.

2.1.2.4 Conclusions for lab-based throughput and latency

We have shown that in addition to the SODALES final-drop application scenario, rate-adaptive optical wireless communications can also provide a low-cost optical alternative to mm-wave radio for small-cell mobile backhauling. We have achieved a record for the bitrate-times-distance product of $14 \text{ Gbit/s}\cdot\text{m}$ with latencies as low as 2 ms using an LED-based link featuring closed-loop real-time link adaptation enabling reliable operation of the link for variable weather conditions. In addition we have learned that homogeneous illumination due to the active area of the LED significantly simplifies the deployment and makes the link more robust against misalignment. Moreover, we have observed that flow control is essential in order to achieve low latency in general at any frame size. Further system improvements, like the latency reduction down to 2 ms with a new chipset, which comes at 230% higher net data rates, indicate that LED-based optical wireless links can also be adapted to the increasing demands anticipated for future mobile radio systems, such as 5G.

2.1.3 Initial field experiments

After the first lab measurements, we have also investigated the potential of LED-based OW fixed final-drop and backhaul links by means of a five-month outdoors trial. Here, we demonstrated that availability is high at common small-cell to macro-cell distances, and that data rates of 1 Gb/s per wavelength are achievable. Statistical analysis is included therefore in the link model and it enables prediction of the achievable data rate statistics for varying environmental conditions. At the end, a link design is proposed for a 1 Gb/s LED-based OW backhaul link suitable also for deployment in the SODALES field-trial demonstration.

2.1.3.1 Setup for the initial field experiments

As shown in Figure 7 (left), both OW systems used in the outdoor trials were encapsulated into a robust, weatherproofed housing. The two transceivers were then installed, one on south front of the Fraunhofer Heinrich Hertz Institute (HHI) building and the other onto the rooftop of the Institute for High Frequency Technology (HFT) of the Technische Universität Berlin (TUB), covering a transmission distance of nearly 100 m. In the same way as for a realistic macro-to-small-cell scenario, there was a difference of 25 m in height, also visible in Figure 7 (right), revealing typical additional effects described in the next sections.

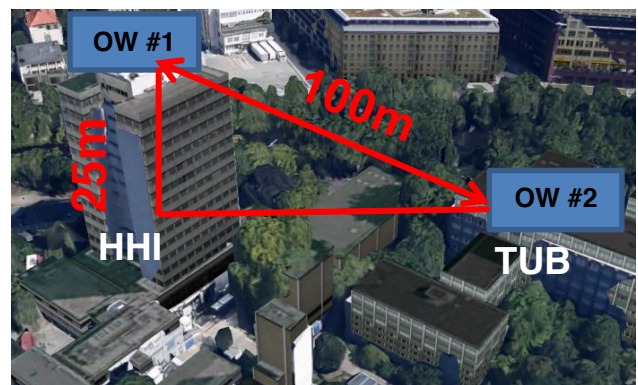


Figure 7: Left: Optical wireless transceiver prepared for outdoor trials. Right: Campus map of TUB where the link is installed (source Google Earth/Berlin 3D).

Simultaneous measurements of the visibility range were made possible by mounting a visibility sensor including a Vaisala PWD12 weather station nearby the OW link at the HHI site. The weather station recorded visibility (up to a maximum of 2000 m) for all types of precipitation and over the whole measurement period. In parallel to the weather conditions, every two minutes, the corresponding link data rates were monitored, in order to observe the behavior of the OW link in realistic outdoor conditions.

Statistics of the visibility and the achieved data rate were calculated from the logged data from which important link parameters such as availability and the minimum data rate and visibility range can be derived.

Besides bad weather events like heavy rain, snow or fog, also the influences of scattered and direct sunlight were observed. Because of the short link distance of 100 m, scintillation caused by atmospheric turbulences may be neglected, as its influence on the link is very low [8].

Outdoor long-term measurements were performed over the winter term (from the end of Nov. 2014 to the end of Jan. 2015). This period is critical for the weather and conditions are better during other seasons of the year. Thus, our measured statistics can be regarded as arising from a worst-case scenario.

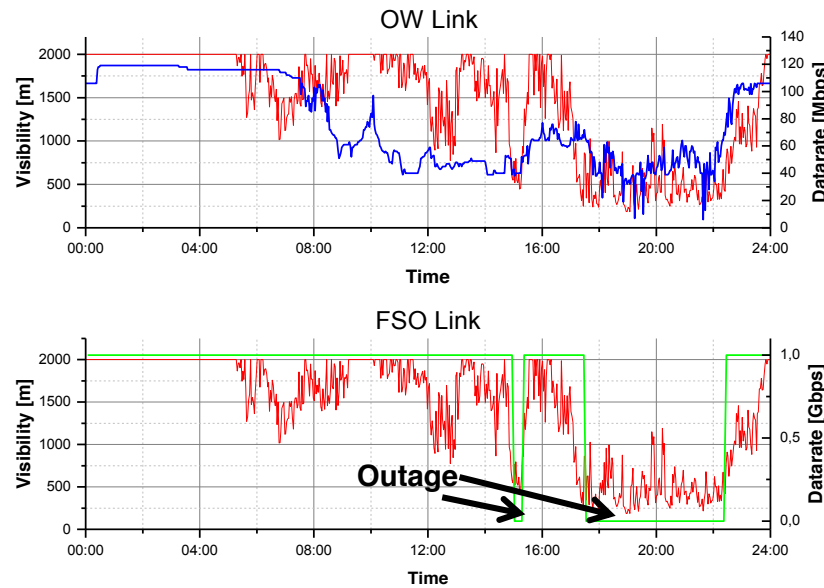


Figure 8: Recorded Visibility (red) and data rate (blue) for the OW link (top) as compared to the FSO link data rates (green curve, bottom) during a dense fog event.

2.1.3.2 Results for the initial field experiments

In Figure 8, results from a dense fog event on December 31, 2014 are presented. Visibilities as low as 250 m were measured, temporarily, posing an extreme challenge for the OW link. With the present configuration and over a distance of 100 m, the OW link achieves a data rate of 120 Mb/s in clear sight conditions. Reduced visibility increases the atmospheric attenuation and the data rate is subsequently reduced so as to maintain a stable link. At some points in time, the data rate dropped down to a minimum value of 9 Mb/s, but the connection was always maintained and available.

For comparison, a 500 m free-space-optical (FSO) link with a fixed data rate of 1 Gb/s located at the same position as the OW link was observed simultaneously. The FSO link is operated at a fixed data rate with a link margin of 12 dB. Hence, atmospheric attenuation due to reduced visibility has no effect unless the margin is fully consumed, which is approximately the case when visibility is lower than the link distance.

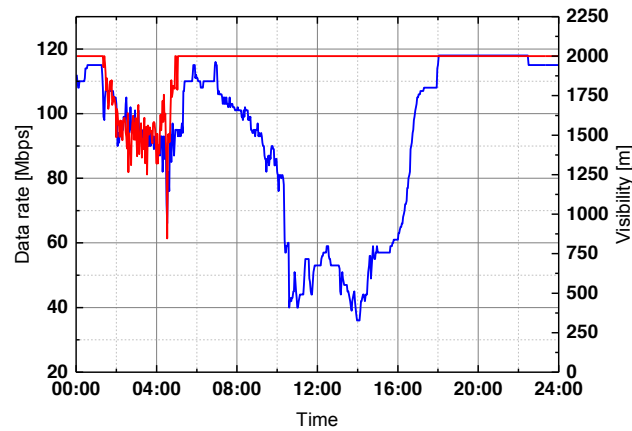


Figure 9: Despite high visibility (red curve) reduced data rates for the OW link (blue curve) are observed for several hours due to sunlight scattered by clouds

However, if the atmospheric attenuation is larger than the margin, the link is interrupted, i.e. communication is no longer possible. Dense fog thus caused an outage event of almost six hours for the FSO link, while our rate-adaptive optical wireless link was always available, albeit at a reduced data rate. Of course, the rate-adaptive OW link is impaired by reduced visibility, e.g. even at visibilities above 2 km, the data rate is reduced due to the missing link margin. Negligible outage is considered mandatory for a reliable backhaul solution, in which case we assume that a reduced rate is an acceptable performance parameter, in contrast to the situation of a link that may be blocked for several hours.

Direct and scattered sunlight

A completely clear or partly cloudy sky is likely to impair the link. With a clear sky and the sun outside the FOV of the receiver, the generated background noise is negligible and so there is no reduction of the data rate. There are, however, a few days of the year when the sun has a very low angle of incidence and directly hits the PD of the receiver for a short time. We have not observed such events so far, because the downward link faced a southerly direction. The second case is a partly cloudy sky, where the sun is illuminating the clouds from behind such that it is only scattered sunlight that is hitting the receiver. As seen in a particular event between 1 p.m. and 5 p.m., on Feb. 18, 2015 in Figure 9, a reduction of the data rate occurs because of such a situation, even though the visibility was good throughout this time. Although best visibility is observed after 7 a.m., the data rate degraded between noon and 3 p.m. The reduced link performance coincides with the sunrise at 7.15 a.m. in combination with a cloudy sky, resulting in a high intensity of the scattered sunlight. Not until the sunset at 5.24 p.m. did the data rate return to its maximum value. Our measurements indicate also that such scattered sunlight events appear in both link directions. This can be explained by the urban environment and nearby buildings reflecting scattered sunlight observed in the FOV of the receiver. The effect of such reflected light was surprising and illustrates the importance of the influence of the surrounding environment.

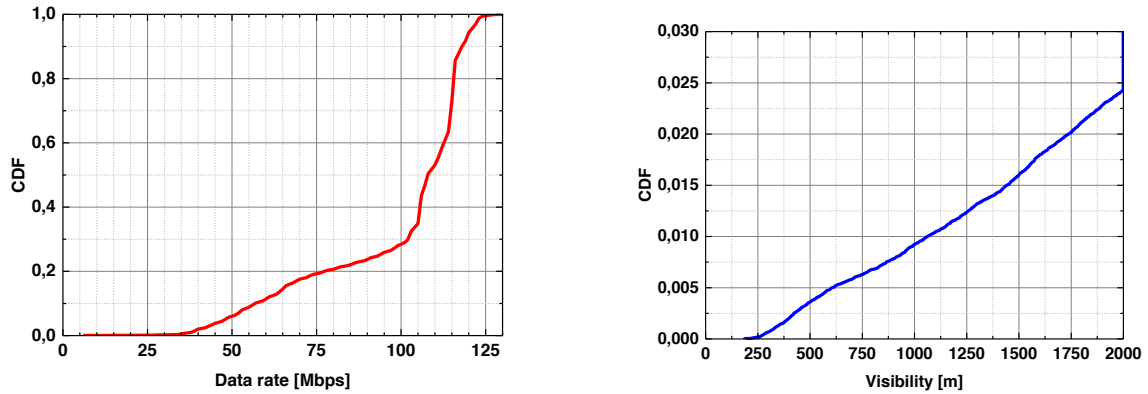


Figure 10: Cumulative distribution function of the observed data rate (left) and the visibility (right)

Note that the receiver used in our experiments was originally designed for visible light communication (VLC) applications having a wide FOV, despite the relatively large lens used here. We assume that the influence of the scattered sunlight can be reduced by reducing the effective area of the photodiode, which also reduces the FOV at the receiver. Further, an optical band-pass filter can reduce the fraction of the sunlight received beside the desired signal. By increasing the directivity at the transmitter, a higher link margin can also be realized. In this way, we anticipate that impairment effects due to the direct and scattered sunlight can be minimized.

Data rate statistics and link availability

Besides instantaneous results regarding the visibility and data rate for given weather conditions, long-term measurements also yield the statistics of the achievable data rate of the OW link. For the appropriate design of an enhanced rate-adaptive OW link, particularly in the SODALES fixed final-drop context, the probability distributions of visibility and data rate are also useful. In Figure 10, the empirical cumulative distribution functions (CDFs) of both the visibility and the data rates of the OW link are shown. These statics have been obtained over the entire measurement period. Our results indicate that the data-rate is higher than 100, 39 and 22 Mb/s in 72, 99 and 99.9 % of all cases. Visibility was never below 200 m. Maximum measurable visibility was 2 km.

Parameter	Value
Wavelength	850 nm
Distance	100 m
Focal Length Transmitter	100 mm
Focal Length Receiver	85 mm
Transmitter Lens Diameter	75 mm

Receiver Lens Diameter	75 mm
LED effective Diameter	7 mm
LED FWHM	12°
Radiant Flux	430 mW
Visibility	10 km
Photodiode effective Diameter	14 mm
Lens Transmittance	0.92
Dark Current	5 nA
Bandwidth	50 MHz
Spectral Background Radiance	2 Wm ⁻² sr ⁻¹ nm ⁻¹

Table 1: Parameters of the current OW link.

As already observed in the instantaneous results, there are deviations between visibility and the achievable data rate due to the sunlight, which have additional effect on the data rate. Snow and rain are also included in how the visibility is measured. Snow can partly block the link, while both snow and rain can partly cover the acrylic glass cover of the transceivers and leave water drops on it - This effect can be reduced with the addition of an appropriate roof shelter. All the possible optimizations of the setup learned so far (more directive transmitter, smaller photodiode area, spectral filtering, sun shield and shelter roof for sun and snow) will combine to materially improve the performance at the lower tail of the statistics of data rate, and also improve the availability of the high data rates.

Measurements have to be continued over a longer period of time in order to obtain the full statistics from which accurate availability statistics can be calculated. Nevertheless, at this lab stage of the SODALES project the results are very promising - the initial statistical results are already giving valuable insights into an improved and more appropriate link design. These results are also indicating the great potential for the rate-adaptive OW technology to be deployed as a backhaul solution over short distances, because the availability was high; this despite all the various impairment effects which were not mitigated for in the experimental outdoor setup. There were no outages in the whole five months of the outdoor trial, and data rates higher than 100 Mb/s were available for almost 80% of the time.

2.1.3.3 System optimization

One of the reasons for measuring the impact of the environmental conditions on the OW link was to include these effects in a theoretical link model. The model simulates the SNR at the receiver for a fixed optical setup, predicts the achievable link capacity and can also include the environmental conditions. By modifying link parameters, the above-mentioned enhancements for

the OW system can be included and their impact predicted so that a next generation OW link setup can be developed.


Focal Length Transmitter	175 mm
Focal Length Receiver	200 mm
LED effective Diameter	1.5 mm
Receiver Lens Diameter	100 mm

Table 2: Optimized key parameters

The parameters of the OW link, shown in Table 1 were first introduced into the model and the model was then calibrated against the current results. Subsequently, the model was used to optimize the system by evaluating the impact of key parameters on the link performance. The optimization aims at increasing the SNR at the receiver by varying key parameters such as the LED effective diameter, transmitter and receiver focal length and the receiver lens diameter. Practical limits were thereby taken into account, since it was very important to obtain a realistic system approach. Table 2 shows the results for the four key parameters. According to these new parameters, the electrical SNR can be increased by 26 dB. This additional margin can be used to improve the availability of the link on the one hand, and/or the throughput of the system on the other hand. As described in [4], the analog LED driver used in the OW link enables a modulation bandwidth of 180 MHz, but the bandwidth is currently limited by the relatively large photodiode. A smaller PD not only reduces the influence of the background light but also positively impacts the system bandwidth. Exploiting this bandwidth will need a chipset to successfully exploit the available bandwidth. Most recent results predict that 1 Gb/s over 100 m can be achieved using an OW link with single-wavelength, low-cost LED and a PD receiver.

2.1.3.4 Conclusions for the initial field experiments

We evaluated the performance of a low-cost rate adaptive optical wireless system with a peak gross data rate of 500 Mb/s to be used as a final-drop technology for the SODALES architecture, or as a backhaul link for small mobile radio cells. An existing link was customized for the desired applications in order to perform initial long-term outdoor trials. A 100 m link distance was monitored over the five most critical winter months to observe the influence of bad weather conditions. Both, visibility and the impact of direct and scattered sunlight were found to be critical. Initial results indicate that the OW data-rate is higher than 100, 39 and 22 Mb/s for 72, 99 and 99.9 % of the time, respectively. The lowest observed data rate was 9 Mb/s. Visibilities lower than 200 m were never observed even for the worst weather conditions, which leads to unprecedented availability, at least over short distances. A link model was developed and key parameters modified indicating that it is possible to achieve 1 Gb/s per wavelength over 100 m distance. Altogether, our results indicate that low-cost optical wireless links are feasible over short distances to offer very high data rates. Therefore, we believe that they can play an important role as final-drop links in the SODALES network as well as in the deployment of many small cells in future mobile radio systems.

	<i>Deliverable D4.2</i>	<table><tr><td>Project</td><td>SODALES</td></tr><tr><td>Doc</td><td>D4.2 Prototype implementation and lab validation</td></tr><tr><td>Date</td><td>9/07/2015</td></tr></table>	Project	SODALES	Doc	D4.2 Prototype implementation and lab validation	Date	9/07/2015
Project	SODALES							
Doc	D4.2 Prototype implementation and lab validation							
Date	9/07/2015							

2.2 Mm-wave fixed links

2.2.1 Introduction

Converged 5G networking is emerging as an important research area in next-generation access architectures. Critical aspects of 5G research are high bandwidths available to end-users (e.g. 1 Gb/s to mobile devices and 10 Gb/s to fixed premises, residential or SMEs), latency (with a target of 1 ms delays), lower energy consumption, and higher security. Towards these targets, the introduction of mm-wave (24 and 60 GHz) technologies into 5G access network architectures is attracting interest, since they act as an enabler for many technical solutions to these requirements. The millimetre-wave bands at 24 and 60 GHz have recently become a major option for shorter-range, high-speed communication systems, with these bands offering multi-Gb/s throughput as required by multimedia consumer-oriented applications such as uncompressed video streaming and kiosk flash-downloading services [6][7], and device-to-device (D2D) and device-to-infrastructure (D2I) functionalities.

The 802.11ad standard was formed in January 2009 to address the newly developing 60 GHz market, with initial applications of 60 GHz technology envisaged to include HDMI cable replacement by transmitting uncompressed HDMI. The WiGig specification, which aims to achieve multi-gigabit wireless communication in the 60 GHz band, has since been contributed to the new 802.11ad amendment. It is built on the existing 802.11 standard where interoperability with the 2.4 GHz and 5 GHz bands are based on the existing 802.11b/a/g/n and the 802.11ac standards. Wilocity and Qualcomm have already demonstrated IEEE 802.11ad based chipsets, and it is anticipated that by 2017, IEEE 802.11ad will be an integral part of many consumer electronic devices such as personal computers, tablets and mobile phones. 802.11ad access points operate at the 60 GHz, which is an unlicensed band available worldwide. Such systems in this frequency region can serve bandwidth hungry applications offering high transmit power and wideband frequency allocations. The basic technology features of the 802.11ac and 802.11ad standards are laid out in Table 1.

The 24-GHz band is designated an instrumentation, scientific and medical (ISM) band and is license-free. As such, it is also attracting growing interest for high-capacity wireless communications, suitable for integration into future 5G networking architectures.

The most widely used standards such as 802.11g and 802.11n standards are not serving many applications. For instance, applications that require greater than 1 Gb/s at ranges of 10m or more a wireless solution did not exist. In recent years, the continued effort in pursuit of gigabit wireless communications has been most noticeable in the IEEE 802.11 WLAN [8]. For example in 2010, the Wireless Gigabit (WiGig) Alliance, formed by a consortium of industry leaders, has completed the first draft of the WiGig specification [9] that defines a unified architecture to enable tri-band communications over the frequency bands of 2.4, 5 and 60 GHz. The millimetre-wave bands at 24 and 60 GHz have recently become a major option for shorter-range, high-speed

	Deliverable D4.2	Project SODALES Doc D4.2 Prototype implementation and lab validation Date 9/07/2015
---	-------------------------	---

communication systems. As opposed to 802.11ac, which is an evolution of 802.11n, 802.11ad was formed in January 2009 to address the newly developing 60 GHz market. The initial applications of 60 GHz technology included HDMI cable replacement by transmitting uncompressed HDMI.

Table 3: Basic technology parameters for 802.11ac and 802.11ad

	802.11ac	802.11ad
Access Technology	Multi-user + Spatial Division Multiplexing / OFDM	Single-user, one spatial stream / Single Carrier or OFDM
Frequency Band	5 GHz	60 GHz
Channel Bandwidth (MHz)	20, 40, 80, 160	2160
Maximum Data Rate (Mbps)	80 MHz, 4 spatial streams: 1733 160 MHz, 4 spatial streams: 3466 160 MHz, 8 spatial streams: 6933	Single Carrier: 4620 OFDM: 6756

The WiGig specification, which aims to achieve multi-gigabit wireless communication in the 60 GHz band, has since been contributed to the new 802.11ad amendment. It is built on the existing 802.11 standard where interoperability with the 2.4GHz and 5 GHz bands are based on the existing 802.11b/a/g/n and the 802.11ac standards. Wilocity and Qualcomm have already demonstrated IEEE 802.11ad based chipsets. It is anticipated that by 2017, IEEE 802.11ad will be an integral part of many consumer electronic devices such as personal computers, tablets and mobile phones. 802.11ad access points operate at extremely high frequency (around 60 GHz). This band is available worldwide and is unlicensed. Such systems in this frequency region can serve bandwidth hungry applications offering high transmit power and wideband frequency allocations.

Figure 11 illustrates the historical physical layer (PHY) data rate improved with these amendments.

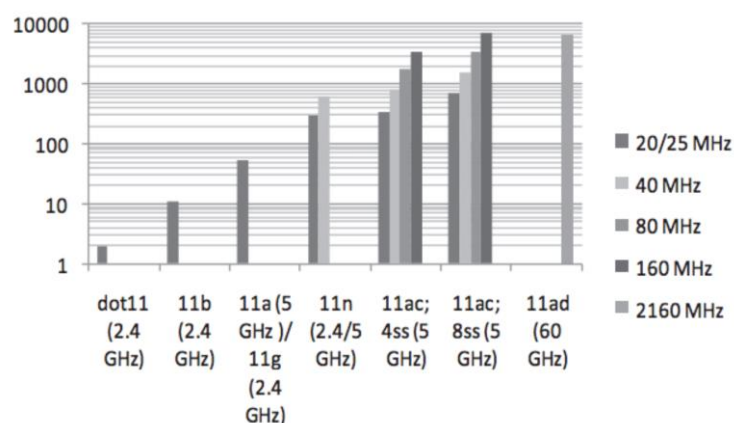


Figure 11: Historical 802.11 PHY data rate improvement

	<i>Deliverable D4.2</i>	<table><tr><td>Project</td><td>SODALES</td></tr><tr><td>Doc</td><td>D4.2 Prototype implementation and lab validation</td></tr><tr><td>Date</td><td>9/07/2015</td></tr></table>	Project	SODALES	Doc	D4.2 Prototype implementation and lab validation	Date	9/07/2015
Project	SODALES							
Doc	D4.2 Prototype implementation and lab validation							
Date	9/07/2015							

2.2.2 IEEE 802.11ac

802.11ac operates strictly in the 5GHz band, but supports backwards compatibility with other 802.11 technologies operating in the same band. As an evolution to 802.11n, 802.11ac adds 80 MHz, 160 MHz and non-contiguous 160 MHz (80 + 80 MHz) channel bandwidths. Another major throughput enhancement feature is multi-user capability in the form of downlink multi-user MIMO (DL MU-MIMO). Furthermore, 802.11ac increases the modulation constellation size from 64 QAM to 256 QAM.

Devices that implement the 802.11ac standard have to be fully interoperable with 802.11g and 802.11n. It is also important that 802.11ac only applies to the 5 GHz band, as there is no room in the 2.4 GHz band for the 80 and 160 MHz channels. Having a backward compatible preamble ensures coexistence with existing 802.11 devices.

In general, 802.11ac could be seen as a lateral extension of 802.11n in which the two basic notions of multiple input, multiple output (MIMO) and wider channel bandwidth, anchored in 802.11n [10][11] are enhanced. The basic idea is that the theoretical maximum PHY data rate can be linearly increased by a factor of the number of spatial streams (transmit/receive antennas) or channel bandwidth. Doubling the number of spatial streams and channel bandwidth can double PHY data rate [12][13].

2.2.2.1 5GHz MU-MIMO

Most wireless networks have multiple active clients that share the available bandwidth. The overall throughput can only be increased by increasing the link rate for all clients. Many clients cannot transmit at the highest 802.11ac rates though because they only have one or two antennas. For such clients, MU-MIMO is the solution to get significant network throughput gains. A MU-MIMO capable transmitter can transmit multiple packets simultaneously to multiple clients as shown in Figure 12 below.

In 802.11ac, a MU-MIMO mode is defined with up to eight spatial streams divided across up to four different clients. For example, in 80 MHz mode it would be possible to send packets to four clients simultaneously at a data rate per client of 866.6 Mb/s, assuming all clients can receive two spatial streams. This means the total data rate of 3.46 Gb/s is four times larger than it would have been without MU-MIMO. The data rate per client is also larger, because the MU-MIMO packets can be transmitted at the maximum data rate per client while without MU-MIMO, each client can only be transmitted to about a quarter of the time such that the effective per-user throughput is a quarter of its maximum. In practice, the throughput gain of MU-MIMO is reduced a bit by the fact that acknowledgments are still sent sequentially in time. Also, depending on the signal-to-noise ratios for all clients, it may not be possible to maintain the maximum data rates in a MU-MIMO packet because a MU-MIMO link does lose some signal-to-noise ratio relative to a single-user link. One of the challenges in launching successful MU-MIMO products will be how to do the link adaptation in an environment with changing numbers of clients and potential switches between single-user and multi-user packets.

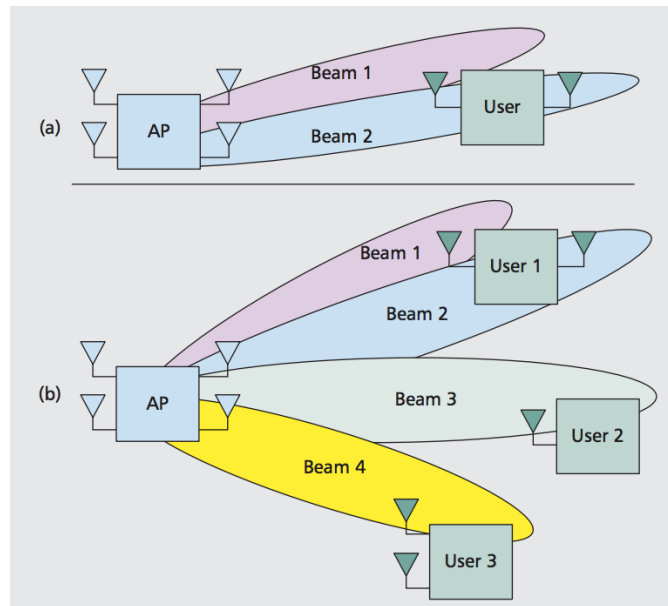


Figure 12: Different MIMO concepts: a) SU-MIMO beamforming; b) downlink MU-MIMO beamforming

Another challenge will be how to deal with time variation in the channel because MU-MIMO requires accurate channel knowledge in order to minimize inter-user interference. The 802.11ac standard specifies a single method of explicit compressed beamforming feedback to enable both MU-MIMO and single-user beamforming. The fact that a single method was picked is expected to help in market adoption and ensuring interoperability. This is in contrast to 802.11n where the presence of multiple feedback options avoided widespread adoption of beamforming

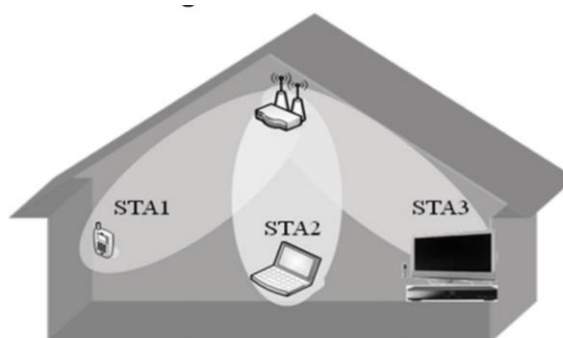


Figure 13: Example of downlink MU-MIMO

The advantage of MU-MIMO is that client devices with limited capability (few or one antenna) do not degrade the network capacity by occupying too much time on air due to their lower data rates.

With downlink (DL) MU-MIMO, network capacity is based on the aggregate of the clients of the simultaneous transmission (Figure 13).

2.2.2.2 LARGER BANDWIDTH

In 802.11n, channel bandwidths of 20 and 40 MHz are defined. In 802.11ac, 2 more bandwidths of 80MHz and 160 MHz are introduced. The 80 MHz mode uses two adjacent 40 MHz channels with some extra subcarriers to fill the unused tones between two adjacent 40 MHz channels as shown in Figure 14 below.

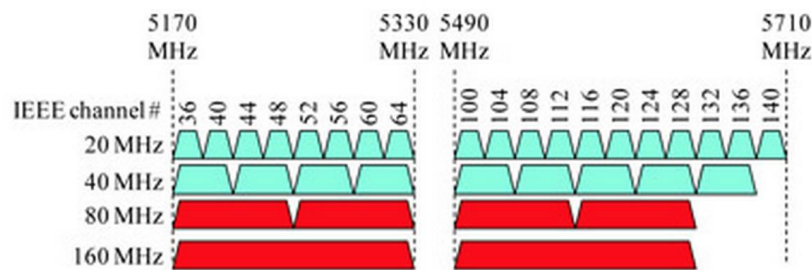


Figure 14: Data channels for 802.11ac in Europe

The 160 MHz mode uses two separate 80 MHz channels without any tone filling in the middle of these two subchannels. In a 160 MHz channel, a data rate of 866.6 Mb/s can be achieved for a single spatial stream using 256-QAM. With the maximum number of spatial streams of eight, data rates up to 6.933 Gb/s are possible [14].

2.2.3 24 GHz Wireless

At present, virtually all 24 GHz wireless systems use either horn or parabolic dish antennas [15][16]. Here, we took advantage of a commercially available 24 GHz point-to-point link wireless system (Ubiquiti airFiber). This system featured both multiple-input-multiple-output (MIMO) technologies, dynamically variable signal constellations, together with adaptive time/frequency multiplexing.

The combination of the best features of both time-division duplex (TDD) and frequency-division duplex (FDD) (e.g., interference-reduction and flexible band-planning) enhances the realization of the specified 1.4-Gb/s delivery as established by the results of the real-time application measurements conducted [17][18]. Typically, dB mm-wave excess path loss might be expected in an open-plan design modern building with large glass windows. In contrast, thick stone walls, small windows, and many internal solid walls will produce losses considerably in excess of this [19]. Also, attenuation by walls, floors, furniture, and scattering are all to be expected in the chosen propagation environment.

Here, we will focus on the emerging 24 GHz unlicensed band and present the first path-loss and basic throughput measurements in the office environment using a 24 GHz point-to-point link.

Even with just 100 MHz available bandwidth, this 24 GHz wireless link can support high bit-rate applications (up to 1.4 Gb/s aggregate) due to reduced interference [20]. Typical application areas could be within public buildings, universities, or hospitals with a range up to 150 m.

2.2.4 802.11ad and WiGig

WiGig and IEEE 802.11ad operate very similarly to 802.11ac but transmits signals in the 60GHz spectrum band, which is widely available for unlicensed use around the world. The technologies offer theoretical maximum data rates of 7 Gb/s with a relatively small transmission range that allows them to work only within a small area. WiGig and 802.11ad will be largely backward compatible with existing Wi-Fi standards.

Because of the amount of bandwidth available in the 60 GHz band, four 2.16-GHz wide channels are used. These are 50 times wider than 802.11n's channels. Transmitting in the 60 GHz band enables WiGig and 802.11ad to offer higher data rates because there is so much bandwidth available in that frequency range. Unlike 802.11ac, WiGig and 802.11ad use beamforming to enable communications over longer distances.

Signal attenuation is high at 60 GHz band therefore the link budgeting is challenging. To improve the signal strength at the receiver, high gain antennas are deployed. These high gain antennas, mostly phased-array antennas, utilize beamforming to create beams in a particular direction allowing the transmitted power to be focused.

Since transmission in the 60 GHz range is subject to greater free-space loss than in the 2.4 or 5 GHz range. The channel conditions can change dramatically during a connection (for example, someone moves between a BluRay player and a projector - human body loss is between 20 and 40dB. This can be managed in real time by using beamforming.

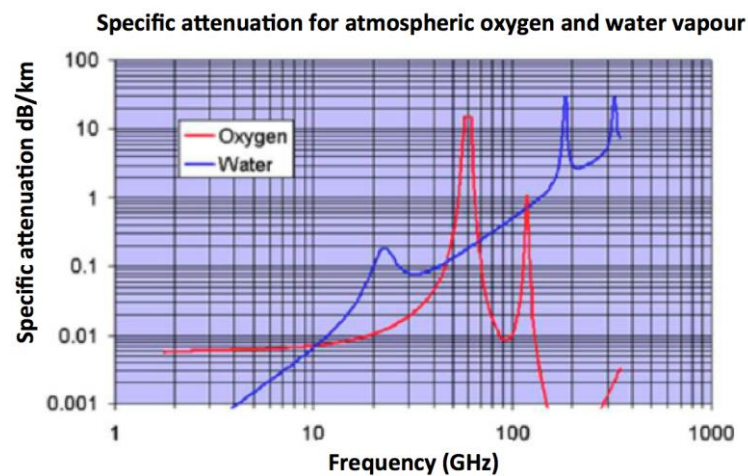


Figure 15: Specific attenuation for atmospheric oxygen and water vapour

At 60 GHz spectrum, radio signals suffer from higher propagation and atmospheric loss compared to 5 GHz as shown in Figure 15. For the same range, free space loss at 60 GHz is 21 dB more than free space loss at 5GHz (e.g., for 1 m range free space loss is 68 dB at 60 GHz, and 47 dB at 5.5GHz). The general rule of thumb is every 6 dB increase in propagation loss halves the coverage distance.

60 GHz chipsets exploit the short-carrier wavelength by incorporating antennas or antenna arrays directly onchip or in-package. Because the antenna size in the 60 GHz band is very compact, small and competitive antenna arrays can be used. 802.11ad supports beamforming in realtime. During the beam refinement process, training sequences for beamforming are sent between the transmitter and receiver and evaluated. The best antenna weightings for each situation can then be set [21].

2.2.4.1 CARRIER FREQUENCY

802.11ad is an amendment to 802.11 for enhancements for multi-gigabit throughput in 60 GHz band. Figure 16 shows the spectrum allocation for unlicensed operation at 60 GHz. In this band, typically 7 GHz of spectrum is available for unlicensed usage compared to 83.5 MHz in 2.4 GHz band.

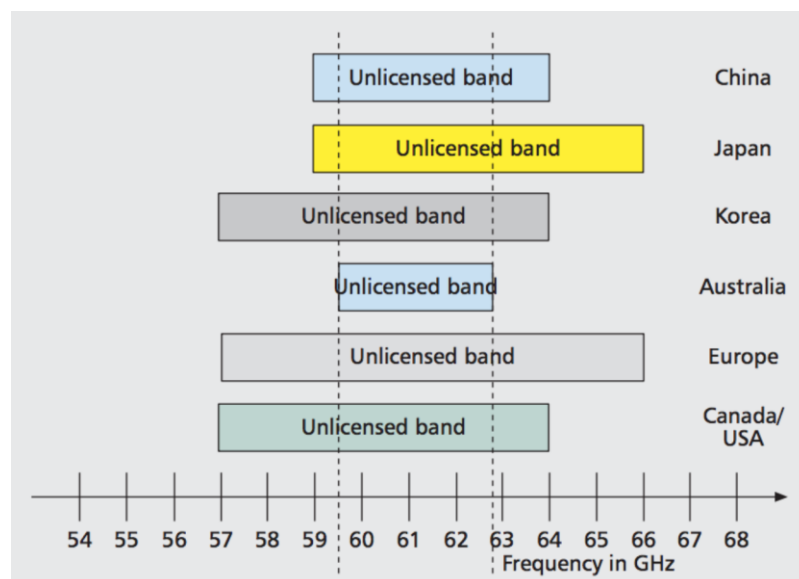


Figure 16: Worldwide frequency allocation at 60 GHz band.

2.2.4.2 MULTI-GIGABIT MODULATION AND CODING SCHEMES

802.11ad defines both single carrier (SC) modulation and OFDM (Orthogonal Frequency Division Multiplexing) modulation. OFDM enables longer distance communication and greater delay spreads. This provides flexibility in handling obstacles and reflected signals.

Single carrier PHY is low on power consumption and focuses on small form factor devices like handsets. SC uses p/2-B/SK, p/2-QPSK, and p/2-16-QAM modulation with the maximum achievable PHY data rate of 4.620 Gb/s [22].

802.11ad PHY data rates range from 385 Mb/s to 6.7 Gb/s, achieved through combinations of modulation scheme and code rate. For the BPSK modulation scheme, PHY data rate achieved by 802.11ad using 2.16 GHz channel bandwidth and 802.11n employing 20 MHz channel bandwidth is 385 Mb/s and 6.5 Mb/s, respectively, i.e., a 58 times increase in the PHY data rate, leveraging larger channel bandwidth. Whereas in 802.11ac it is based on sending more bits per symbol (256-QAM) and use of simultaneous data streams (up to 8), because bandwidth is limited to a maximum of 160 MHz as discussed earlier [11].

Table 4: Channel numbers in the 60 GHz band.

Channels	
1	58.32 GHz
2	60.48 GHz
3	62.64 GHz
4	64.80 GHz


Four channels are defined for this band as shown in Table 4 above, but they are not universally available. Channel 2 is available in all regions and is therefore used as the default channel.

2.2.5 802.11ac and 802.11ad implementation and suitability for multi-gigabit use

Complementary metal oxide semiconductor (CMOS) technology is used for fabrication of WiFi transceivers. 2.4/5 GHz band WiFi transceivers can be synthesized with more conventional CMOS technologies, which are cheaper, whereas 60 GHz WiFi transceivers can only be synthesized with state-of-the-art CMOS technology (65 nm, 40 nm, etc.) As of today, 40 nm CMOS technology is expensive, thus making 802.11ad transceivers more costly than 802.11ac transceiver.

Considering the challenges discussed above, an important question is raised. Are 802.11ac and 802.11ad suitable for the same type of applications, or there are preferred classes of applications for each one?

IEEE 802.11ac is suitable for longer-range high-throughput applications, such as in-home wireless LAN and compressed multimedia wireless display. While 802.11ac seems to be more appropriate for longer-range applications, the transmitter power regulatory and power consumption requirements limit the applicability to the different use cases. Since the obstruction loss at 5 GHz is lower than at 60 GHz, multi-gigabit 802.11ac is more appropriate for both line-of-sight and non-line-of-sight wireless applications where portability is not a bottleneck. 802.11ac

	<i>Deliverable D4.2</i>	<table><tr><td>Project</td><td>SODALES</td></tr><tr><td>Doc</td><td>D4.2 Prototype implementation and lab validation</td></tr><tr><td>Date</td><td>9/07/2015</td></tr></table>	Project	SODALES	Doc	D4.2 Prototype implementation and lab validation	Date	9/07/2015
Project	SODALES							
Doc	D4.2 Prototype implementation and lab validation							
Date	9/07/2015							

chipsets are already being deployed in mobile phones, PCs, laptops, and mobile devices. Phones use the technology for higher-speed networking, watching HD video, and videoconferencing.

Obstruction loss is significant at 60 GHz as it was mentioned earlier. Therefore, 802.11ad is more appropriate for line-of-sight, room-scale, low-cost, short-range, very-high-throughput applications, such as in room uncompressed and lightly compressed multimedia wireless display, sync data/file transfer, and so on. 60 GHz high gain antennas with low cost and small size can also be realized for point-to-point applications such as small-cell backhaul networks. Despite lower propagation loss at 5 GHz band, strict regulatory requirements limit the transmit power proportional to the transmitter antenna gain. Thus, range extension required for backhaul networks cannot be achieved at 5 GHz.

WiGig and 802.11ad chipsets will be used mainly with UHD TVs and consumer electronics, to enable the transmission and transfer of data intensive high-definition signals. The technologies could also be deployed in mobile phones, laptops, and even peripherals such as printers. The first application that already demands these technologies are streaming or copying movies to a hard drive or video monitor from Blu-ray discs wirelessly, rather than over an HDMI cable.

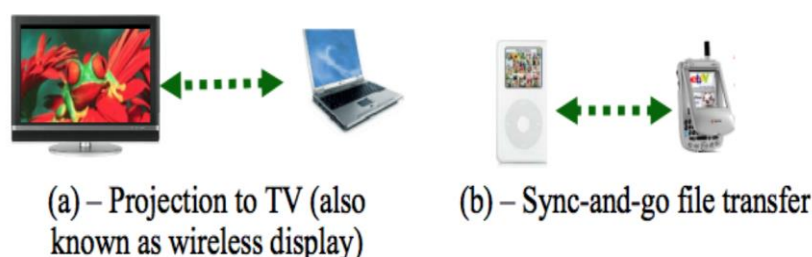


Figure 17: Example scenario of 802.11ad [14]

The 60 GHz spectrum is also known as the “oxygen absorption band”, as it was mentioned earlier, That means, radio waves at those frequencies are actually degraded by the presence of oxygen in the air. For this reason, 60 GHz was considered only appropriate for point-to-point, outdoor applications using highly directional antennas (e.g., wireless links between two networks). It could also be used in outer space for inter-satellite communications where oxygen is obviously not a problem, or for indoor short-range applications, such as linking device docks with wireless interconnects, as shown in Figure 17 above.

2.2.6 Experimental results

2.2.6.1 802.11AC POINT-TO-POINT

Our results have shown that for connection distances 802.11ac offers significantly improved performance compared to 802.11n in a typical office environment, with data rates up to 940 Mb/s for a 3 × 3 MIMO configuration as shown in Figure 18 below.

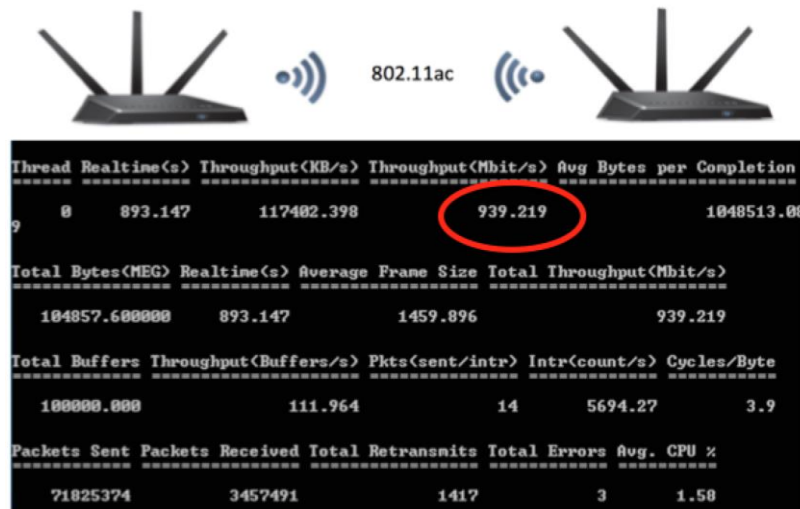


Figure 18: 802.11ac point-to-point experimental results.

However, these performance improvements are sensitive to channel conditions, with the achieved data rates rapidly declining as the distance between the transmitter and the receiver is increased.

2.2.6.2 24 GHz POINT-TO-POINT

The test system consisted of the 24GHz point-to-point link with maximum output of 20 dBm. It had a 1.4-Gb/s aggregate capacity using hybrid division duplex (HDD) in bidirectional mode with a 64 QAM modulation scheme. This could be dynamically reduced to QPSK through automatic rate adaptation with lower signal-to-noise ratios (SNRs). This feature enabled the link pair to sustain up to 142.5 dB path loss when switched to basic QPSK modulation mode. The transmitting and the receiving terminals had an antenna gain of 33 dBi each.

Both antennas were mounted on tripods 1.7 metres above the floor level and connected to PCs for signal transmission monitoring. The wireless network setup was taken to three different location scenarios for measurement of signal strength and throughput capacity under LOS and NLOS propagation situations.

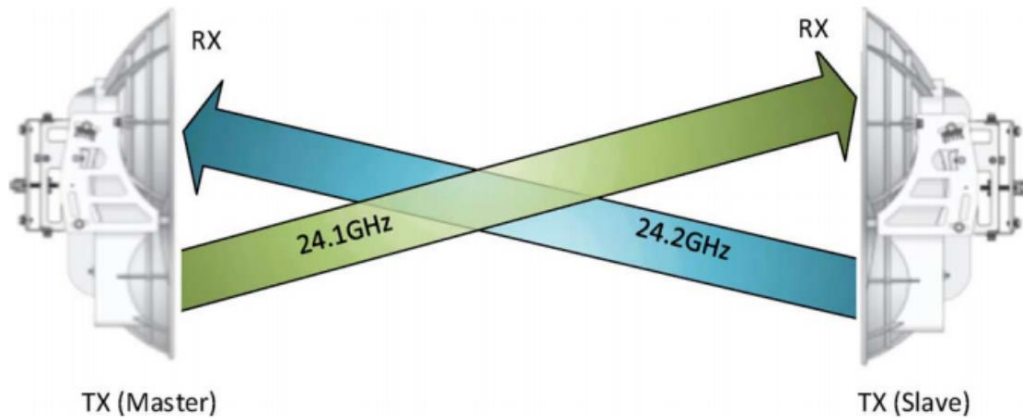


Figure 19: GHz back-to-back set-up in full duplex operation [23].

Figure 19 above shows the setup of the Ubiquity Air Fibre 24GHz point-to-point links transmitter and receiver [23]. Both the transmitter and receiver were mounted on modified camera tripods. The received signal in the beam steering case was relatively stable; this could have been due to multipath and reflections effects.

A data rate of 743 Mb/s was recorded in bidirectional transmission of the link with the system operating at carrier frequencies of 24.1 and 24.2 GHz in full-duplex mode.

The aggregation of the two channels -transmission of 743 Mb/s and receive of 743 Mb/s simultaneously- lead to a total of 1.4 Gb/s. Signal strengths of around 67 dBm were recorded at a Tx–Rx separation of 46m.

Thickness (mm)	Material	Attenuation dB
5	Plexiglas	3
8	Perspex	3
11	Plywood	4
13	Delrin	2
1.5	Plastic sheet	2
3	Hard board	3
5.5	Plywood	2
6.3	Tufnell	2

Table 5: Attenuation of various building materials

24GHz as compared to 60GHz to penetrate walls between offices in a modern building, hence WLAN deployed on this frequency band can be used for multimedia applications and gigabits required services in offices. Table 5 shows the attenuation of various building materials.

2.2.6.3 QUALCOMM (WILOCITY) COMPLETE 802.11AD SOLUTION

UEssex has several examples of this technology as part of the Dell Latitude laptop offering. Data rates of ~3 Gbit/s are possible over distances of ~20 metres. All standard interfaces are provided so uncompressed 4k UHDTV signals were transmitted.

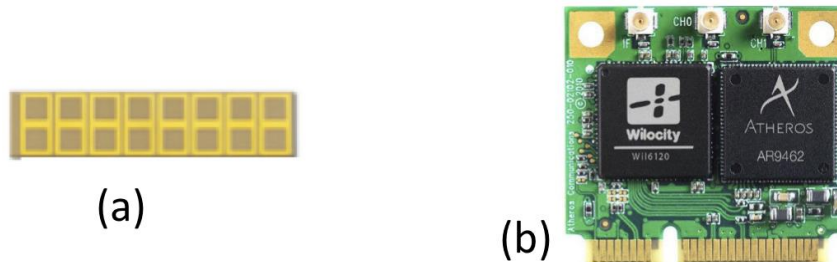


Figure 20: (a) Active antenna, (b) Wireless card [24]

Figure 20(a) is an active antenna module while Figure 20(b) shows the tri-band (2.4/5/60 GHz) half mini-card used in the laptop implementation. The functionality of the antenna and radio card is documented in a series of patents; granted and pending [25]. On inspection, a technically advanced beam steering antenna is revealed with functionality and sophistication on a par with that of SiBeam. This appears to be the world-leading pure RF technology at present.

The Latitude 6430u laptop was placed at a constant distance of 2 metres away from the Dell wireless WiGig dock D5000 802.11ad access point (AP) placed at the centre with the angular variation of 0 to 360 degrees, as shown in Figure 21.

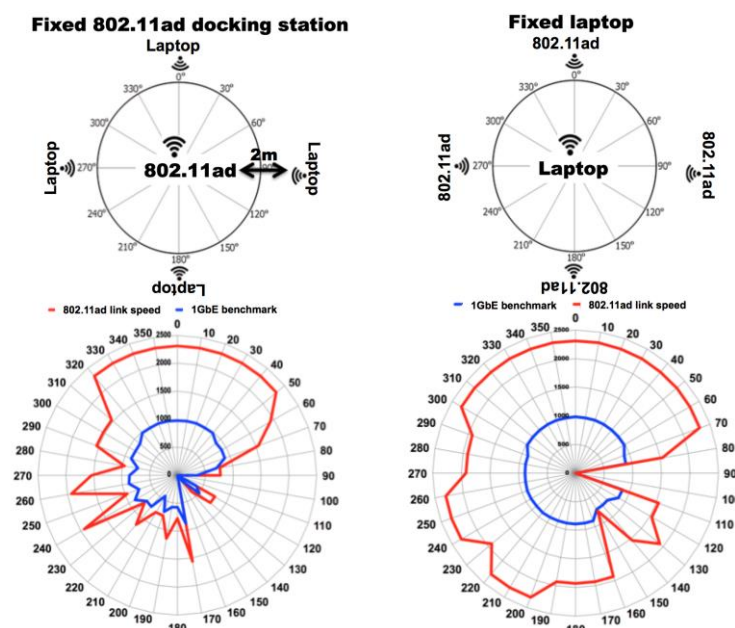


Figure 21: Omnidirectional antenna basic characterisations (left: 90° azimuth directivity, right: 330° azimuth directivity)

The connection was maintained when the laptop was moved around the dock. However, the link speed (<2.4 Gb/s) and the maximum wired 1GbE throughput (<980 Mb/s) was not constant which is due to the characteristics of the omnidirectional antennas in both the dock and in the Latitude.

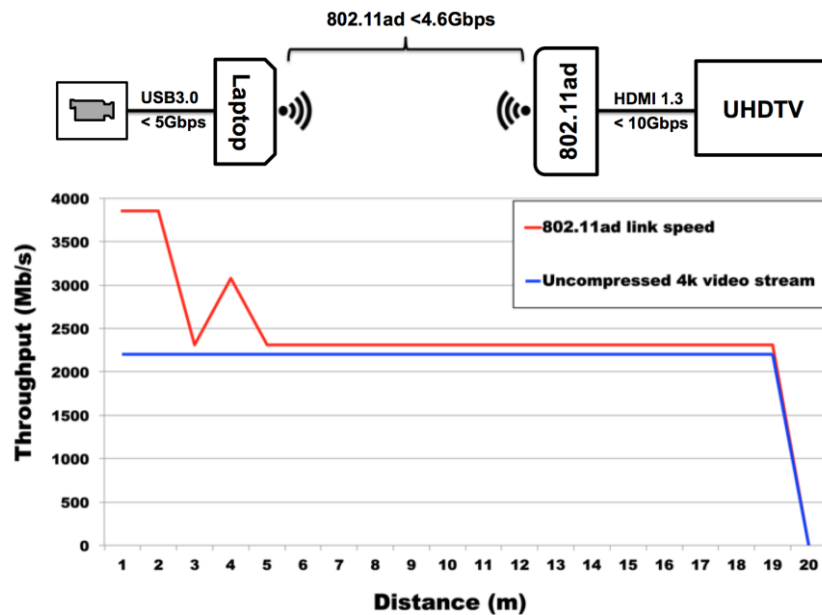


Figure 22: Live streaming of 4K UHD TV signals over 802.11ad

The next experiment focused on increasing the range of the wireless link. Figure 22 shows the dell docking station to Latitude wireless setup at 60GHz frequency for a delivery of 4K uncompressed video stream from the 4K camera to the UHD TV display.

It was found that the wireless link can be maintained for longer than 10 metres in distance, as shown in Figure 22. The operation of the wireless link was extended to about 19 metres in an indoor environment where a line of sight connection was achieved. The results presented here show that for full signal strength and maximum throughput (~2.3 Gb/s) the docking station must be in line of sight with the Latitude. It was also found that polarization plays a critical role during multi-channel transmission in the 60 GHz waveband that should be considered for the possible aggregation of 802.11ad links.

2.2.6.4 DUAL-POLARIZATION PATCH

Studies at Essex University (UEssex) have centred on full, end-to-end system realizations with the transmit/receive antennas being integral components. A first example is a linear/horizontal polarization-switched resonant patch antenna as shown below in figure 16.

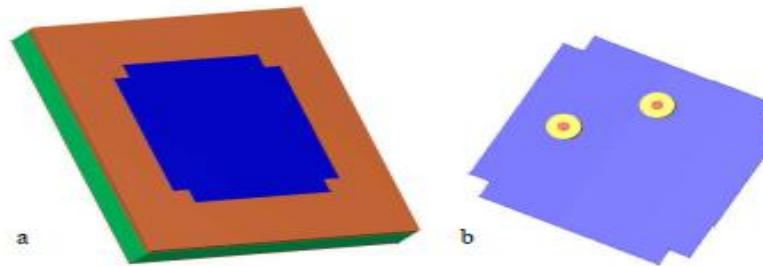


Figure 23: (a) Antenna structure, and (b) Patch feed points

The design was simulated with CST Microstripes software as shown in Figure 24 below.

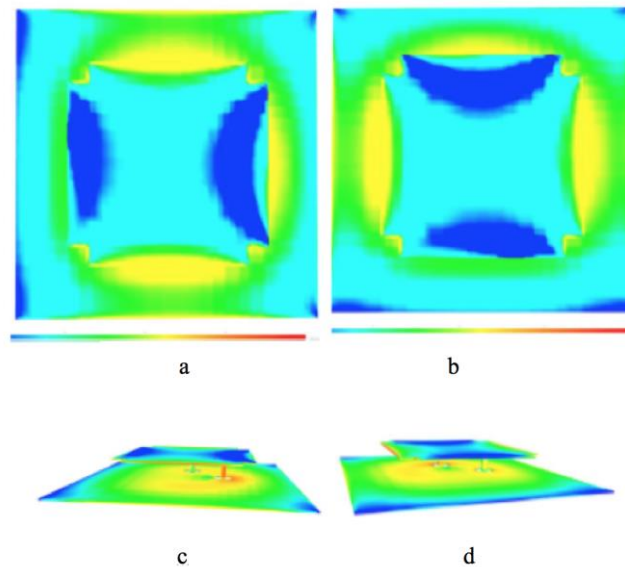


Figure 24: (a) Port 1 excited for horizontal polarization. (b) Port 2 excited for vertical polarization. (c) Port 1 side view. (d) port 2 side view

As shown, the patch resonant effect is clearly delineated and, in this case, offered 1.5 GHz bandwidth centred on 5 GHz with 8 dBi gain and a maximum 44.6 dB S_{11} value. Figure 25 shows the physical embodiment. The broad bandwidth band was due, in part, to the use of Eccostock PP-2 material.

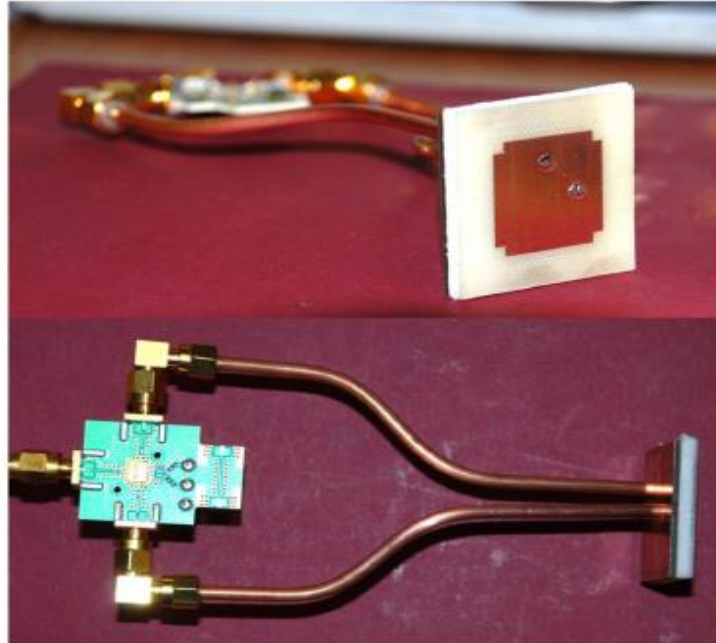


Figure 25: 5 GHz H/V polarization patch and MMIC switch.

In consequence, the patch $\lambda/2$ width was 21.62 mm against a free-space value of 30 mm at 5 GHz including an allowance for fringing effects. It should be noted that the patch centre frequency is directly scalable, subject to the aforementioned fringing effects. For example, a 40 GHz patch would have ~3.7 mm unconstrained resonant width. Higher frequencies still become limited by fringing effects.

2.2.6.5 LEAKY FEADER

UEssex have constructed micro- and mm-wave leaky-feeder antenna with encouraging results. Figure 26 below shows a novel, 60 GHz, slotted, semi-rigid cable-based antenna with 15.3 dBi gain [26].

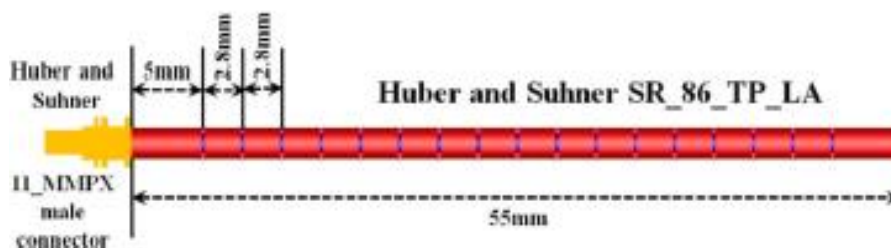


Figure 26: 60 GHz semi-rigid slot antenna [26].

The slots were laser ablated to form Babinet dipoles. As can be seen, the slot spacing was carefully chosen in the sub- $\lambda/2$ region to avoid grating lobes. Self-apodization across the 55mm span removed the need for any end termination [26].

The radiation patterns shown in Figure 27 below highlight the quasi-discoidal radiation pattern and also the “squint due to end-feeding.

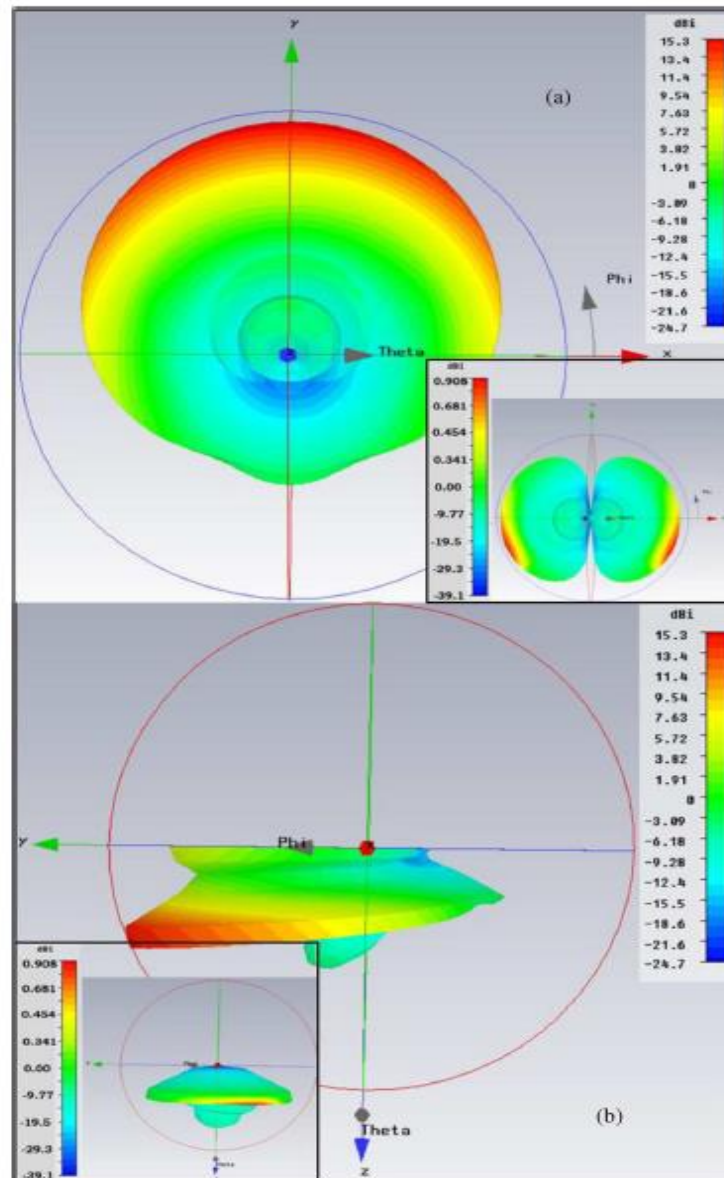



Figure 27: Copolar E-plane radiation patterns at 60 GHz (corresponding crosspolar radiation patterns inset): (a) top view and (b) side view.

Recent simulation work on up to quad arrays of these antennas has shown a close approach to the expected 6 dBi gain enhancement.

	<i>Deliverable D4.2</i>	<table><tr><td>Project</td><td>SODALES</td></tr><tr><td>Doc</td><td>D4.2 Prototype implementation and lab validation</td></tr><tr><td>Date</td><td>9/07/2015</td></tr></table>	Project	SODALES	Doc	D4.2 Prototype implementation and lab validation	Date	9/07/2015
Project	SODALES							
Doc	D4.2 Prototype implementation and lab validation							
Date	9/07/2015							

2.2.7 5 Gbit/s Realtime Baseband Processing

Future converged fixed-mobile networks need high-speed radio links in deployment scenarios where fibre is not available or too expensive. We present a field-programmable gate array (FPGA)-based real-time transmission system using standard 10G Ethernet interfaces. The system comprises two parallel complex-valued data channels in each direction. Standard FPGAs and low-cost multi-channel analogue-to-digital converters (ADCs) and digital-to-analogue converters (DACs) have been used. For enhanced robustness and optimal usage of the power amplifier, $\pi/4$ -shift differential quaternary phase-shift keying (DQPSK) modulation is used. All digital signal processing routines for synchronization, equalization, forward error correction etc. have been fully implemented and tested. Using a protocol analyzer, error-free bidirectional transmission of Ethernet frames at 5 Gbit/s is verified. Error-vector magnitude (EVM) values below -30 dB indicate that even higher speeds could be realized.

2.2.7.1 Introduction

The increasing demand for higher data rates in fixed and mobile networks needs the deployment of optical fibre, which is, however, not always available. In order to bridge such missing links wirelessly, commercial radios support 1 Gb/s. The main limitation towards even higher data rates is the baseband signal processing, as the range above 1 Gb/s is not yet covered by existing chipsets. Here we describe the real-time implementation of the complete physical layer signal processing chain for a bidirectional 5 Gb/s mm-wave link on a reconfigurable FPGA platform using low-cost DAC and ADC. The intention is to demonstrate that all required algorithms can be implemented in parallel on commercially available FPGA and that practical solutions can be found where this is not possible, like for initial frame synchronization and in case of hardware impairment effects, like AC-coupled baseband inputs. This section of the Deliverable D4.2 is organized as follows; first the real-time system is described, then the challenges faced during implementation are discussed, and finally the system performance is presented.

2.2.7.2 System Description

System Overview

Each transceiver contains a 5 Gbit/s transmission and reception part composed of two parallel 2.5 Gbit/s transmitters and receivers respectively. Each transmitter/receiver requires two analog outputs/inputs in order to process the complex-valued $\pi/4$ -shift DQPSK signals in in-phase (I) and quadrature (Q) component. A block diagram of the required digital signal processing functions is shown in Figure 28. These blocks comprise standard IP Cores (e.g. Reed Solomon encoder/decoder), straightforward implementations of commonly used functions (e.g. scrambler/descrambler) and resource-efficient as well as novel algorithm implementations (e.g. frame synchronization, DC compensation). The following sections describe the main digital signal processing blocks in detail with special emphasis on real-time implementation challenges.

Ethernet/Flow control

An essential feature of the system is its ability to adjust the incoming Ethernet traffic to the actual system capacity. The data rate that can be processed at the transceiver is currently limited by the sample rate of available low-cost DACs and ADCs. With sample rates of 2.5 GSa/s per transmitter/receiver and an oversampling factor of two a maximum rate of 1.25 GBd per channel can be achieved with the $\pi/4$ -shift DQPSK format. Moreover, an overhead of approximately 6.45% due to FEC coding and training sequence insertion sets the net data rate to approximately 4.6 Gbit/s in each direction. In order to avoid packet loss, delays, or even data corruption flow control is mandatory. It is realized by using the backpressure mechanism according to the IEEE 802.3x standard. Pause frames indicate to the sender how long the transmission has to be stopped or whether it can be restarted.

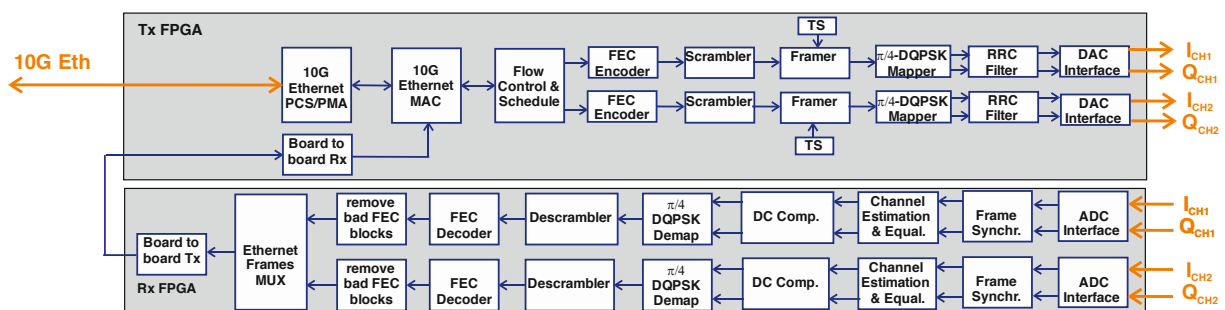


Figure 28: Real-time transceiver building blocks

Coding, modulation, and filtering

The Ethernet stream is distributed in two parallel channels that are encoded by a Reed-Solomon FEC (255,239) and scrambled using a 15 bit linear feedback shift register (LFSR). Then a training sequence is periodically inserted before modulation. For enhanced robustness and reduced peak-to-average power ratio compared to standard DQPSK, $\pi/4$ -shift DQPSK modulation is used [27]. The complex symbols are up-sampled by a factor of two and pulse shaped by a root-raised cosine (RRC) filter with a roll-off factor of 0.5. Finally, the resulting samples are forwarded to the DACs.

Frame Synchronization

One of the biggest challenges has been the implementation of a frame synchronization algorithm able to process high data rates. Since FPGAs usually run at clock rates in the order of 200 MHz, processing of samples in the GSa/s-range is only possible by parallelization. Here, each 2.5 GSa/s stream is divided into 16 parallel streams that are processed at a clock rate of 156.25 MHz.

The well-known Schmidl and Cox algorithm [28] has been used for frame synchronization. In order to process 16 samples in parallel the original Schmidl and Cox algorithm would have to be parallelized e.g. as proposed in [29]. However, such a parallel structure prevents to benefit from the algorithm's inherent iterative computing and consumes much more FPGA resources than the

serial approach. Therefore, we have chosen a serial implementation together with an off-line like signal processing to take advantage of the low training sequence periodicity (Figure 29).

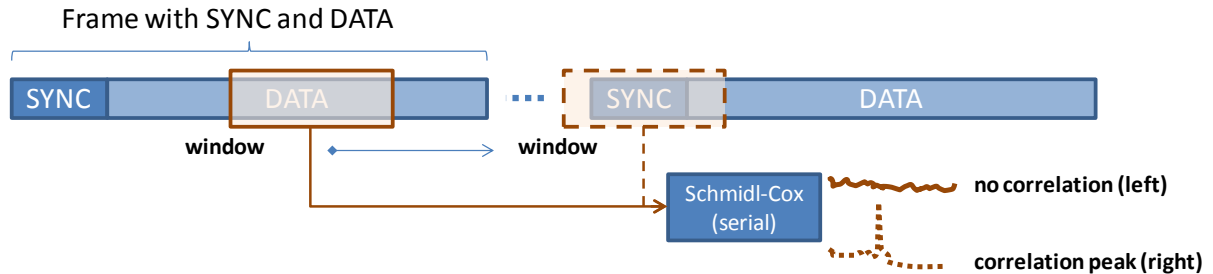


Figure 29: Frame synchronisation using the serial Schmidl-Cox algorithm of a continuous data stream

Instead of running the algorithm continuously over the whole data stream, only a short window of samples is captured and processed in a serial manner. The calculation of the Schmidl-Cox algorithm is finished well before the next window is captured. If the SYNC sequence at the beginning of the frame was not found, the capture window is shifted by half of its size for the next frame and so on. Finally the window contains the SYNC sequence completely and a correlation peak is detected. For the following frames the window position is adjusted, so that the SYNC sequence is in the center of the window. A drawback of this method is that it can occasionally take longer to find the very first frame start after the link is established or interrupted. However after the initial lock the synchronization becomes rapidly stable and the system remains locked in normal operation. Right after synchronization, the training sequence is also used for channel estimation and equalization. The feed-forward add-and-overlap frequency-domain equalizer is also described in [30].

DC-Compensation

When the system is not completely DC-coupled, the $\pi/4$ -shift DQPSK modulation format cannot handle repetitive patterns like they may appear in long Ethernet frames. In the implemented system the DACs have a wide-band transformer with a band pass behavior from approximately 4.5 MHz to 3 GHz. A scrambler and a descrambler have been implemented in the transmitter and receiver respectively in order to minimize the appearance of such repetitive patterns. A simple compensation algorithm was implemented to compensate the observed DC-drift. This algorithm calculates the offset between symbol and constellation point for every fourth symbol and applies it to correct the following four symbols. Then the offset is calculated again. In Figure 30 the effect of the band-pass characteristic can be seen. In the left diagram an end-to-end simulation without scrambler is shown. The baseline drift causes an error floor when the DC compensation algorithm is not used (left pointing triangle). When the DC-compensation algorithm is being used an error-free transmission is possible again. A penalty of ~ 4 dB at $\text{BER} = 4 \cdot 10^{-4}$ compared to theoretical curve (dashed line) can be observed for this case. When in addition the scrambler is

being used the penalty decreases slightly to ~ 3.5 dB, because the repetitive pattern is randomized by the scrambler (right figure).

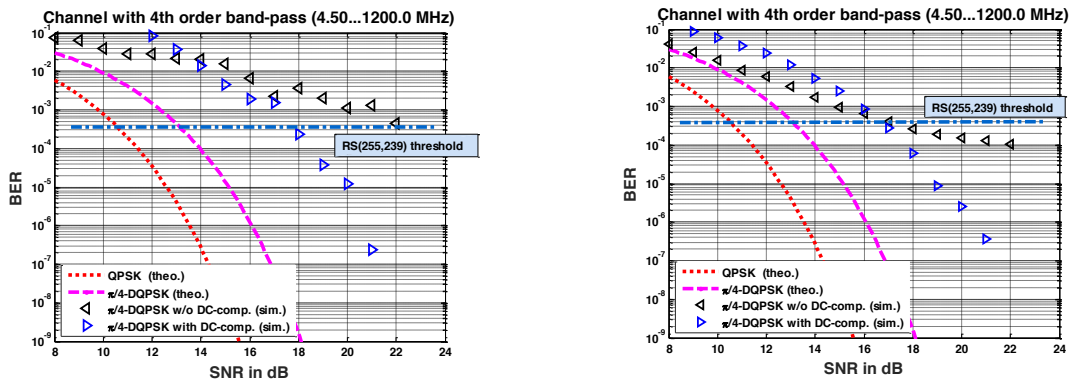


Figure 30: BER simulation with and w/o DC-compensation (left w/o scrambler, right with scrambler)

The equalized and DC-free signal is then $\pi/4$ -shift DQPSK demodulated, descrambled and processed by the FEC decoder. At this point the Ethernet frames can be recovered and both channels are multiplexed into a single Ethernet stream that is sent back to the transmission part where the 10G Ethernet interface is implemented.

2.2.7.3 Transceiver hardware

Two development boards are used for the implementation of each transceiver, one FPGA for the transmission part and one FPGA for the reception part. The transmission board is connected to two dual-channel 2.5 GSa/s DAC boards by two FPGA Mezzanine Card (FMC) connectors as well as to an SFP+ board in order to provide the 10G Ethernet interface. Similarly, two dual-channel 2.5 GSa/s ADC boards are connected to the reception board by two FMC connectors.

2.2.7.4 Experimental setups

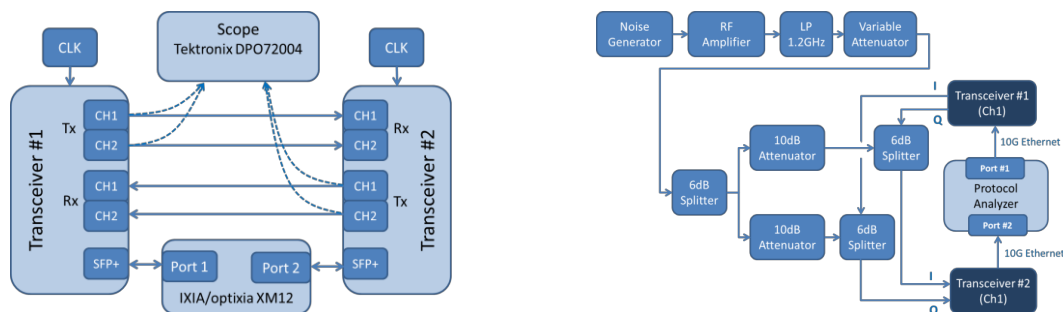


Figure 31: Setups for packet loss ratio (a, cont. lines), EVM (left, dashed) and SNR vs BER (b) measurements

To analyze the system performance different tests have been performed. The EVM was measured using the setup shown on the left in Figure 31 with dashed lines. Data was captured

using a Tektronix scope and post-processed in Matlab. A balanced test pattern was used, so that each $\pi/4$ -shift DQPSK constellation point was used with the same probability, the RRC filter was bypassed. The test pattern was internally generated in the FPGA. As shown on the left in Figure 31 with continuous lines, the packet loss ratio was measured with a protocol analyser and with the transceiver in electrical back-to-back configuration and independent clocks. The BER versus SNR was measured as shown on the right side in Figure 31. A noise generator together with an RF amplifier and a low pass filter was used as a noise source for the analogue signals. The noise between I and Q was uncorrelated by increasing the cable length of one channel (I) by 20 cm. With a variable attenuator the noise level was controlled while the signal level remained constant. To compute the BER extra logic was built in the receiver FPGA to gain information from the FEC decoder and count the number of corrected bits.

2.2.7.5 Experimental results

Physical Layer

Figure 32 shows the result of the transmitter output characterisation for one transceiver. EVM values below -30 dB were obtained, which indicate that even higher speeds than 5 Gbit/s could be realized. The measured BER over SNR is shown in Figure 5. The noise and signal level at the receiver input was the same for I and Q and the maximum signal power was used for this measurements. The BER curve before FEC has been achieved by evaluating the number of corrected FEC blocks (block size: 8). The curve after FEC has been calculated by means of detected frame errors by the protocol analyser. It should be noted, the theoretical curve is before FEC. The implemented system achieves error-free transmission (BER = 10^{-9}) for SNR ~ 15.5 dB.

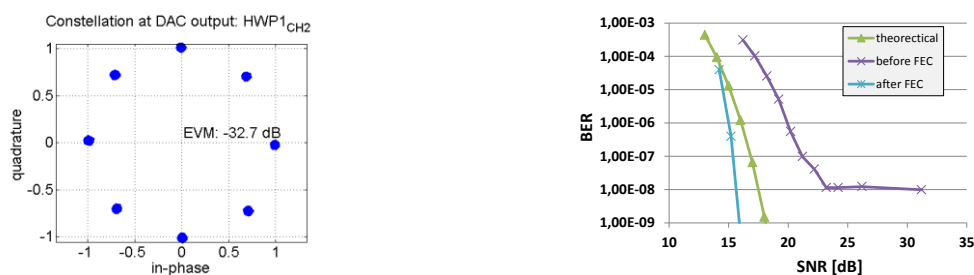


Figure 32: Constellation plot and EVM results (l.), Bit Error Ratio vs Signal to Noise Ratio (r.)

Ethernet results

In Table 1 the main protocol analyser parameters, measured during a test of approximately 10 minutes, are listed. A bidirectional 5 Gbit/s (net 4.633 Gbit/s) transmission is achieved. All transmitted frames have been received by the other port together with the pause frames sent for flow control purpose. Moreover no errors or losses have been registered, e.g. like frame undersize, oversized or errors in the cyclic redundancy check (CRC) field.

Table 6: Ethernet protocol analyser results

Protocol analyser parameter	Port1	Port 2	Unit
Frames Send	461.709.867	459.574.383	Frame
Send Rate	4,633	4,633	Gbit/s
Valid Frames Received	465.172.141	467.254.863	Frame
Flow Control Frames Received	5.597.758	5.544.996	Frame
Errors (CRC/Undersize/Oversize)	0	0	Error

Conclusions and further work

We compared two standards namely, IEEE 802.11ac and IEEE 802.11ad, which are proposed for 60 GHz short range communication. We provided a brief account of these standards in terms of the local area network (LAN) context. However, their applicability for the ARN final-drop as a fixed-link high capacity wireless technology solution is clear.


The standards were compared on the basis of different schemes proposed for robust wireless connectivity at 5 GHz, 24 GHz and 60 GHz.

Wi-Fi products based on next generation gigabit per second 802.11 technologies are emerging on the market to address use cases that demand higher throughput. 802.11ac evolved in the 5GHz bands with wider channels and multi-user capability to address broader coverage use cases typical of Wi-Fi devices, such as higher resolution video coverage around the home.

Rather than only improving single link throughput by using more bandwidth and 256-QAM, 802.11ac also improves network throughput by adding MU-MIMO capability. MU-MIMO makes it possible to achieve large throughputs cost effectively by having relatively simple client devices with just one or two antennas that can be simultaneously transmitted to by an access point that may have up to eight antennas.

The 24 GHz spectrum described here delivered full-duplex data rates of beyond 1 Gb/s in NLOS conditions. It was demonstrated that gigabit throughput using the 24-GHz frequency band is an option for future in-building wireless networks.


IEEE 802.11ad has emerged, as the choice for Gb/s wireless LAN because of its back compatibility with earlier standards. 802.11ad addresses personal area networking use cases new to 802.11 such as wireless docking with multi-gigabit per second links based on large amount of available spectrum in the 60 GHz band. 802.11ad makes use of directional antennas and beamforming to enhance link quality, and modifies channel access to address directionality and spatial reuse. The relatively limited range of 60 GHz enhances frequency reuse which might even augment overall wireless security because eavesdroppers outside a given installation will have a much more difficult time grabbing 60 GHz signal.

	<i>Deliverable D4.2</i>	<table><tr><td>Project</td><td>SODALES</td></tr><tr><td>Doc</td><td>D4.2 Prototype implementation and lab validation</td></tr><tr><td>Date</td><td>9/07/2015</td></tr></table>	Project	SODALES	Doc	D4.2 Prototype implementation and lab validation	Date	9/07/2015
Project	SODALES							
Doc	D4.2 Prototype implementation and lab validation							
Date	9/07/2015							

It is also believed that mm-wave communications at or around 60 GHz will become an integral part of 5G networks in indoor and outdoor environments. Its integration with the existing lower frequency networks requires considerable efforts at PHY and MAC layers. Already existing 60 GHz research and standardizations can be helpful in defining new schemes for 5G networks.

Finally, we have demonstrated a 5 Gbit/s custom solution for future converged fixed-mobile networks. The presented system is FPGA-based and comprises two parallel complex-valued data channels in each direction together with a standard 10G Ethernet interface. A DSP function to compensate for a lower cut-off frequency of 4.5 MHz has been simulated and implemented. A serial Schmidl-Cox algorithm to perform the frame synchronisation for a 2.5 GSa/s data stream has been shown. The transmitter output signal can achieve EVM values below -30 dB and the required SNR for an error-free transmission was about 15.5 dB. On the Ethernet layer all frames could be transmitted without CRC or other errors.

The baseband data rate of 2.5 Gbit/s per channel could be increased by newly available FMC carrier cards with integrated 5 GSa/s ADC/DAC and additionally by increasing the modulation order from 2 to 4 bits/symbol. With these methods 10 Gbit/s per channel could be achieved.

	<i>Deliverable D4.2</i>	<table><tr><td>Project</td><td>SODALES</td></tr><tr><td>Doc</td><td>D4.2 Prototype implementation and lab validation</td></tr><tr><td>Date</td><td>9/07/2015</td></tr></table>	Project	SODALES	Doc	D4.2 Prototype implementation and lab validation	Date	9/07/2015
Project	SODALES							
Doc	D4.2 Prototype implementation and lab validation							
Date	9/07/2015							

3 Control & Management Platform

Besides the different technological experiments performed at the data plane in the lab trial, this chapter describes the basic features of the control and management platform in order to implement basic fault management within the SODALES architecture, i.e. including both the ARN and the CPE devices. These features cover the fault management requirements gathered at the beginning of the project for the SODALES software platform.

The different fault management features presented in this chapter are considered at the management plane level, from the perspective of alerting the infrastructure and service providers to the different failures that can occur.

3.1 Fault Management

Deliverable D3.1 [31] included the initial overview for the advanced SODALES software-defined management plane. It stated that the control and management plane implements the required operation functions that allow network providers to configure the network, and to offer tailored infrastructure slices to the service providers. In addition, it also enables the OAM of the network services that are deployed on top of each one of the network slices.

Deliverables D3.3 and D3.4 [32][33] presented, respectively, the complete software design and the stand-alone prototype of the SODALES management plane, including both the OpenNaaS-based toolset for the infrastructure provider and the service provider.

In order to provide complete OAM features at both levels, fault management was included in the list of requirements, so the software management platform is capable of providing a set of functions designed specifically for this purpose. Fault management can be defined as the component within network management concerned with detecting, isolating, and even resolving problems [fault-management]. Fault management provides measures in order minimize network downtime.


In the SODALES management plane, fault management has been mainly focused on event detection in the ARN, and implementation of the CFM standard features for the CPE related services. The next sub-sections contain the description of the prototypes for fault management in both the ARN and the CPE.

3.1.1 Active Remote Node

The ARN is the fundamental device within the SODALES architecture. In order to ensure network performance and correct status, it is fundamental that the required alarms, events, and status monitoring is implemented in the management platform for the ARN.

Two distinct mechanisms ensure the full knowledge over the operational GPON network status:

- Asynchronous Notifications for some events

	<i>Deliverable D4.2</i>	<table><tr><td>Project</td><td>SODALES</td></tr><tr><td>Doc</td><td>D4.2 Prototype implementation and lab validation</td></tr><tr><td>Date</td><td>9/07/2015</td></tr></table>	Project	SODALES	Doc	D4.2 Prototype implementation and lab validation	Date	9/07/2015
Project	SODALES							
Doc	D4.2 Prototype implementation and lab validation							
Date	9/07/2015							

- Polling Status Information on the different provisioned entities (e.g. Interfaces or Services);

Asynchronous notifications at the ARN devices are handled with a proprietary implementation of the acknowledgment protocol, which is completely integrated in the SNMPv2 agent at both the Network Element and the PTIN private Network Management System. This protocol defines that every notification message should be acknowledged by the NMS, thus the agent at the device should resend a notification each couple of seconds until it is acknowledged.

The focus in SODALES is on the polling mechanisms implemented and included in the open-source release of the management plane.

3.1.1.1 Notifications logging

In order to improve the analysis of problems that may have occurred in the recent past, notifications logging has been implemented. With this, it is possible to consult the past alarms that occurred either on each board or on global system. Only a limited set of alarms are stored in the device due to obvious storage capacity reasons. The different codes utilized for the alarms are further detailed in the Annex A of section 3.1.1.6.

The REST interface specification attached to the physical and virtual resource representations of the ARN is as follows; as well as an example of the view in the management plane (refer to Figure 33).

Request

```
/request/operation [@type="show" AND @entity="alarmRegister"]/alarmRegister
[@equipmentId="value"]
```

Response

```
/response/operation/alarmRegisterList
```

Notifications logging

id	Code	Access Type	Start or End	TimeStamp	LocalTimeStamp	Interfaceld
0	16	0	0	1420645490	1430333231	
1	12	0	1	1420645537	1430333231	262145
2	99902	0	0	1420645574	1430333231	
3	110050	0	0	1420645585	1430333231	
4	36868	0	1	1420645585	1430333231	8781824
5	36868	0	1	1420645585	1430333231	8781824
6	36866	0	1	1420645585	1430333231	8781824
7	12	0	1	1420645585	1430333231	262145
8	12	0	1	1420645585	1430333231	262145
9	36868	0	1	1420645586	1430333231	8781824
10	36868	0	1	1420645586	1430333231	8781824
11	36866	0	1	1420645586	1430333231	8781824
12	36868	0	1	1420645466	1430333231	8781824

Figure 33: Notifications logging view from the unified management plane

3.1.1.2 Equipment information

The status information is essential for diagnosis of the system performance. The ARN provides status information for the most important entities in the system (boards, interfaces, services, among others).

The REST interface specification of the equipment information for the ARN, both physical and virtual, is detailed below. Figure 34 depicts an example of the information for available cards in one physical ARN included in the system.

Request

```
/request/operation [@type="showStatus" AND @entity="card"]/card[@equipmentId="value" AND @id="value"]
```

Response

```
/response/operation/cardList/card/status
```

Equipment Boards - Board status

id	Name	Type	Temperature	CPU Usage	Memory Usage	Storage Usage
0	unknown	0				
1	XCO-160	20211	3600	922	3478	3437
2	UMX-4x10GE	20189	2750	260	6161	3840
3	AMX-48GE	20199	3500	3570	5999	8764
4	AMX-48GE	20199	3600	3528	5996	8699
5	XCO-160	20211	3700	831	2602	2569
6	FAN	20212				

Figure 34: Equipment boards, board status view

3.1.1.3 Switch fabric protection status

There is a specific interface to retrieve the current status information of the available switch fabrics present in the ARN, either virtual or physical. Typically the infrastructure provider uses this feature; although it may be possible for the service provider to receive a virtual ARN with a complete switch fabric. The REST API attached to the resources is specified in the following box.

Request

```
request/operation [@type="showStatus" AND
@entity="matrixStatus"]/matrixStatus[@equipmentId="value"]
```

Response

```
/response/operation/protection/matrixStatusList
```

Figure 35 depicts an example of the output of the aforementioned request in the unified management plane view.

Switch Fabric Status

Switch Fabric status							
Slot ID	Status	FW Status	Software		Data		Commands
			Version	Upgrade Status	Database	Configurations	
1	Active	OK	v3.4.1	---	---	---	--- / --- / ---
5	Standby	OK	v3.4.1	---	Updated	Updated	activate / --- / ---

[Refresh](#)

Switch Fabric Protection Status

Network Service Id	Status
8781824	0

10 25 50 100

Figure 35: Switch fabric status

3.1.1.4 Interface Status

There is also a specific interface to retrieve the information status of the interfaces of the ARN. The implementation has been completed for LAG internal, Ethernet, and GPON interfaces. The REST interface which enables to retrieve the information of a given system interface is specified in the following box.

Request

```
/request/operation [@type="showStatus" AND @entity="lag"]/lag
[@equipmentId="value" AND @cardId="value" AND @ifIndex="value"]
```

Response

```
/response/operation/interfaceList/interface/lag/status
/response/operation/interfaceList/interface/lag/lagMemberPort/ lagMemberPortList/status
```

Figure 36 depicts an example of the status for the LAG internal interfaces.

LAG Interfaces Status

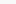
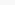

LAG Interfaces					
LAG ID	ETH Ports	Admin	Link Status	Channel Type	Statistics
LAG 1	Slot: 1/ETH 1 	enabled		Static	view
	Slot: 5/ETH 1 				
<div>Refresh</div>					

Figure 36: Lag Interfaces status

3.1.1.5 Service Usage

Finally, there is one more specific interface, which enables one to retrieve information and status (including failures) of the corresponding configured and provisioned services. The REST interfaces which enables the SODALES architecture to retrieve and show the status of the different network services is presented below.

Request

```
/request/operation  [@type="showStatus"  AND  @entity="networkService"]/networkService
[@equipmentId="value" AND @serviceId="value"]
```

Response

```
response/operation/networkServiceList/networkService/stat
```

Figure 37 depicts an example of the view with two network services created, configured and enabled for SODALES, in order to connect one client at the ARN side with one client at the CPE side. It is worth mentioning that this specific service view only shows the services in the ARN.

Services

Counters																								
ID	Service	Ethernet / LAG	PON																slot		Detail			
			1	2	3	4	5	6	7	8	1	2	3	4	5	6	7	8						
			9	10	11	12	13	14	15	16	9	10	11	12	13	14	15	16						
1	<div>SODALES</div>	LAG 1 <div><div></div><div></div></div>	---								---								3	<div><div></div><div></div></div>	<div>Expand</div>			
2	<div>SODALESMultica</div>	LAG 1 <div><div></div><div></div></div>	---								---								3	<div><div></div><div></div></div>	<div>Expand</div>			
<div>Refresh</div>																								

Figure 37: Services list

3.1.1.6 Annex A – ARN Codes

The following tables contain the complete description of the alarm codes for the different ARN system notifications. The codes are provided by the ARN and the management plane utilizes them to inform about the alarm happening at the current time. The ARN codes are only functional for the particular devices implemented within SODALES.

Code	Entity	Description
3	Board	Board has been removed
4	Board	Board is in conflict (a different type of card is expected)
7	Interface	SFP Fail
11	Equipment	Loss of connectivity with the ONU
12	Equipment	48V present
13	Equipment	Temperature alarm
16	Equipment	System boot
18	Interface	Loss of signal (LOS)
26	Interface	Signal Degrade
50	Equipment	Synchronism reconfiguration
79	Interface	Ethernet Link Down
235	Equipment	Mismatch of FW version between the two switch fabrics
296	Board	FAN fail
372	Equipment	Switch fabrics handover due to protection scheme
403	ONU	ONU Loss of signal (LOSi)
404	ONU	ONU Loss of frame (LOF)
405	ONU	ONU Loss of PLOAM
406	ONU	ONU Drift of Window
407	ONU	ONU Signal Fail
408	ONU	ONU Signal Degraded
409	ONU	ONU Loss of GEM channel delineation
410	ONU	ONU Remote Defect Indication (RDI)
411	ONU	ONT Start-up Failure
412	ONU	ONU Loss of Acknowledge
413	ONU	ONU Deactivate Fail
414	ONU	ONU Physical Equipment Error
415	ONU	ONU Receive Dying-Gasp
416	ONU	ONU Transmission Interference Alarm
417	ONU	ONU Video Output Below Threshold
418	ONU	ONU Video Output Above Threshold
419	ONU	ONU Received 1490nm optical power below threshold
420	ONU	ONU Received 1490nm optical power above threshold
421	ONU	ONU Transmit optical power below lower threshold

422	ONU	ONU Transmit optical power above upper threshold
423	Interface	LAG Active Member Down
425	Interface	Signal Fail
426	Interface	Laser End of Life pending
435	ONU	ONU upgrade FW error (no file was found for that particular hardware version)
447	Board	Board entered the “busy” state.
451	Equipment	LOMF detected on synchronism junction number one
452	Equipment	LOMF detected on synchronism junction number two
542	Equipment	LOS detected on synchronism junction number one
543	Equipment	LOS detected on synchronism junction number two
556	Interface	The input power of the EDFA is below the minimum threshold
557	Interface	The input power of the EDFA is above the maximum threshold
558	Interface	No signal was detected in the input EDFA
559	Interface	The output power of the EDFA is below the minimum threshold
560	Interface	The output power of the EDFA is above the maximum threshold
561	Interface	EDFA transmission fail
562	Interface	The EDFA temperature is below the minimum threshold
563	Interface	The EDFA temperature is above the maximum threshold
1002	Board	New board was detected
1006	ONU	ONU FW upgrade (indicates success or fail)


3.1.2 Customer Premises Equipment

The CPE is one of the devices included in the SODALES architecture in order to provide the termination point at the customer premises for network connectivity. Deliverable D3.2 [34] contains the whole specification of the OAM parameters considered with the management plane.

Fault management at the CPE has been prototyped by means of the implementation of elemental Connectivity Fault Management (CFM) features. CFM is further specified in the IEEE 802.1ag standard, where it is emphasized the usage of CFM for Metro Ethernet services.

CFM partitions the service network into various administrative domains, with the major features of the CFM being [35]:

- Fault monitoring using the continuity check protocol. This is a neighbour discovery and health check protocol that discovers and maintains adjacencies at the VLAN or link level.
- Path discovery and fault verification using the linktrace protocol. Similar to IP traceroute, this protocol maps the path taken to a destination MAC address through one or more bridged networks between the source and destination.
- Fault isolation using the loopback protocol. Similar to IP ping, this protocol works with the continuity check protocol during troubleshooting.

	Deliverable D4.2	<div> <div>Project</div> <div>SODALES</div> </div> <div> <div>Doc</div> <div>D4.2 Prototype implementation and lab validation</div> </div> <div> <div>Date</div> <div>9/07/2015</div> </div>
---	-------------------------	--

CFM is supported by the different CPEs. A simplified graphical user interface have been integrated into the management platform for the different providers in order to configure CFM-related parameters through the XML-enabled web service interfaces completely specified and implemented in the deliverable D3.4 [33][36].

display enet table

policer parameters

profile number

CIR

CBS

EIR

EBS

service parameters

service number

source port

policer id

pmid

ingress type

incoming outer vlan

outgoing outer vlan

dest port

edit flow type

edit outer command

swap

continuity check measurement parameters

stream number

ccm activate ☐

destination mac

vlan id priority

source port

md level

cfm version

ccm period

remote indication ☐

meg name

loss measurement ☐

remote mep id

local mep id

policer id

incoming service id

outgoing service id

looback parameters

stream number

lb activate ☐

destination mac

vlan id priority

source port

md level

cfm version

policer id

prbs ☐ inject-error ☐

lb side

delay measurement parameters

stream number

dm activate ☐

destination mac

vlan id priority

source port

md level

cfm version

policer id

lb side

Figure 38: CFM configuration at the ENET CPEs

	<i>Deliverable D4.2</i>	<table><tr><td>Project</td><td>SODALES</td></tr><tr><td>Doc</td><td>D4.2 Prototype implementation and lab validation</td></tr><tr><td>Date</td><td>9/07/2015</td></tr></table>	Project	SODALES	Doc	D4.2 Prototype implementation and lab validation	Date	9/07/2015
Project	SODALES							
Doc	D4.2 Prototype implementation and lab validation							
Date	9/07/2015							

4 Conclusions

In this deliverable D4.2, we have summarised the laboratory testing of the key wireless final-drop interfacing technologies (mm-wave and optical) which will feature in the validation and commercial field tests in the final months of the SODALES project, as well as the fault management system that has been developed for the ARN and CPE components of the SODALES architecture. The key performance indicators, such as 1-10 Gb/s bandwidth capacities over at least 100 metres have been shown to be both theoretically as well as experimentally possible, and over a range of atmospheric conditions. The simulations and modelling results have also indicated where improvements in the technical performance of the technologies can be achieved, e.g. for the optical wireless link, so as to fully satisfy all the specifications of a full commercial deployment as well as for future 5G applications.

This deliverable accompanies the parallel deliverable D4.3, which describes the required installation parameters for the field service validation, following the successful laboratory verification of the technologies described here. Together, these two WP4 deliverables are providing the necessary technical inputs into the final phase of the SODALES project, to ensure a successful commercial field trial conclusion to the project, which will be reported upon in the final WP4 deliverable of D4.4 (M36).

5 References

- [1] T. Nakamura, et al. "Trends in Small Cell Enhancements in LTE Advanced", IEEE Communications Magazine, Feb. 2013
- [2] I.I. Kim, et al. "Availability of Free Space Optics (FSO) and hybrid FSO/RF systems", Optical Wireless Communications IV, SPIE Vol. 4530
- [3] L. Grobe et al. High-speed visible light communication systems, IEEE Communications Magazine, Vol. 51, No. 12, Dec. 2013, pp. 60-66.
- [4] Langer, et al. "Rate-adaptive visible light communication at 500Mb/s arrives at plug and play", <https://spie.org/x104653.xml>
- [5] Next Generation Mobile Networks Alliance, "Next Generation Mobile Networks Beyond HSPA & EVDO", Version 3.0, Dec. 5th 2006
- A. Prokeš, Modeling of Atmospheric Turbulence Effect on Terrestrial FSO Link, Radioengineering, Vol. 18, No. 1, April 2009
- [6] H. K. Pan, "Dual-polarized Mm-wave phased array antenna for multi-Gb/s 60 GHz communication," in Proc. IEEE APSURSI, 2011, pp. 3279–3282.
- [7] P. Smulders, "60 GHz radio: Prospects and future directions," 2003
- [8] G. Hiertz, D. Denteneer, L. Stibor, Y. Zang, X.P. Costa, and B. Walke. The IEEE 802.11 universe. IEEE Communications Magazine, 48(1):62– 70, January 2010.
- [9] Wireless Gigabit Alliance. Defining the future of multi-gigabit wireless communications. White Paper, pages 1–5, 2010.
- [10] IEEE 802.11n 2009. Part 11: Wireless LAN medium access control (MAC) and physical layer (PHY) specifications, Amendment 5: Enhancements for higher throughput. October 2009.
- [11] E. Perahia and R. Stacey. Next Generation Wireless LANs: Throughput, Robustness, and Reliability in 802.11n. Cambridge University Press, The Edinburg Building, Cambridge, UK, 2008.
- [12] L. Cariou et al, Evaluation of saturation of the 5 GHz band, IEEE 802.11- 10/0846
- [13] L. Cariou, P. Christin, 80MHz and 160MHz channel access modes, IEEE 802.44- 10/0385
- [14] IEEE 802.11ad: Defining the Next Generation Multi-Gbps Wi-Fi
- [15] A. C. T. Workings, "Hardware and solution for the broadband wireless industry," Electronic Article, 2013.
- [16] S. Kavanagh, "An introduction to 24 GHz," Electronic Article, 2001.
- [17] S. Yun et al., "Hybrid division duplex system for next-generation cellular services," IEEE Trans. Veh. Technol., vol. 56, no. 5, pp. 3040–3059, Sep. 2007.
- [18] Y. J. Sang, J. M. Park, S.-L. Kim, and K. S. Kim, "An overlaid hybrid division duplex OFDMA system with multihop transmission," ETRI J., vol. 33, p. 201, 2011.

- [19] "XST-AN010a. 6," Digi. Application Note, 2012
- [20] G. Solution, "Ubiquity airfiber 24 GHz point-to-point radio," Electronic Article, 2012.
- [21] IEEE: IEEE Std 802.11ad™-2012. Part 11: Wireless LAN Medium Access Control (MAC) and Physical Layer (PHY) Specifications Amendment 3: Enhancements for Very High Throughput in the 60 GHz Band
- [22] http://cdn.rohdeschwarz.com/pws/dl_downloads/dl_application/application_notes/1ma220/1MA220_1e_WLAN_11ad_WP.pdf
- [23] Oladunni Juliet Femi-Jemilohun, T. Quinlan, Stuart D. Walker, "An Experimental Investigation Into GbE Wireless Data Communication at 24 GHz in Non-Line-of-Sight and Multipath Rich Environments" in IEEE ANTENNAS AND WIRELESS PROPAGATION LETTERS, VOL. 13, 2014
- [24] <http://wilocity.com/products/reference-designs>
- [25] <http://www.faqs.org/patents/assignee/wilocity-ltd/>
- [26] T. Quinlan, S. Walker "A Coaxial, 60-GHz, 15.3-dBi Slot Antenna Array", *IEEE Antennas and Wireless Propagation Letters*, Vol.13, 2014
- [27] V. Jungnickel, et al.: Localized SC-FDMA with Constant Envelope. IEEE 24th International Symposium on Personal Indoor and Mobile Radio Communications (PIMRC). Proceedings. pp. 24-29, 2013
- [28] T. M. Schmidl, D. C. Cox.: Robust Frequency and Timing Synchronization for OFDM, IEEE Transactions on Communications, vol. 45, no. 2, pp. 1613-1621, Dec. 1997.
- [29] N. Kaneda, et al.: Real-Time 2.5 GS/s Coherent Optical Receiver for 53.3-Gb/s Sub-Banded OFDM, Journal of Lightwave Technology, vol. 28, No. 4, pp. 494-501, Feb. 2010.
- [30] R. Elschner et al, "Experimental demonstration of a format-flexible single-carrier coherent receiver using data-aided digital signal processing," Opt. Express Vol. 20, no. 27, p. 28786 (2012).
- [31] SODALES deliverable D3.1, http://www.fp7-sodales.eu/download/public/WP3/SODALESDeliverable3_1FINAL.pdf
- [32] SODALES deliverable D3.3 http://www.fp7-sodales.eu/download/public/WP3/SODALESDeliverable3_3FINAL.pdf
- [33] SODALES deliverable D3.4,
- [34] SODALES deliverable D3.2 http://www.fp7-sodales.eu/download/public/WP3/SODALESDeliverable3_2FINAL.pdf
- [35] Available Online. Retrieved 2015-04-22.
<http://searchnetworking.techtarget.com/definition/fault-management>
- [36] Available Online. Retrieved 2015-04-25.
http://www.juniper.net/documentation/en_US/junos13.3/topics/concept/layer-2-802-1ag-ethernet-oam-cfm-overview-mx-solutions.html